Wiley
Journal of Chemistry
Volume 2024, Article ID 5758810, 24 pages
https://doi.org/10.1155/joch/5758810

WILEY

Research Article

Effect of Green Additives in Copper Electrorefining Bath: Current Efficiency and Surface Characterization Investigation

F. M. A. Abouzeid[1] **and S. Alshammery**[2]

[1]*Chemistry Department, Faculty of Science, Alexandria University, Alexandria, Egypt*
[2]*Department of Basic Engineering Science, College of Engineering, Imam Abdulrahman Bin Faisal University, Dammam, Saudi Arabia*

Correspondence should be addressed to F. M. A. Abouzeid; fatma.abouzeid@yahoo.com

Received 4 April 2024; Revised 30 October 2024; Accepted 25 November 2024

Academic Editor: Ajaya Kumar Singh

Copyright © 2024 F. M. A. Abouzeid and S. Alshammery. This is an open access article distributed under the Creative Commons Attribution License, which permits unrestricted use, distribution, and reproduction in any medium, provided the original work is properly cited.

The copper electrorefining performance in acidified copper sulfate solution utilizing the potential-dynamic polarization technique was established. This was inspected through measurement and comparison of limiting current-cathode potential relationship in a solution of regularly rising methanolic extract concentrations (from 50 to 1000 ppm) of *Lablab purpureus* (*Dolichos lablab*), Linseed (*Linum usitatissimum*), Sidr leaves (*Ziziphus spina-christi*), and Indian costus (*Saussurea costus*). The impact of temperature on the copper electrorefining kinetic was studied. There is a reduction in the limiting current values via developing plant extract concentration while there is a growth in limiting current values via temperature boosting (293–313 K). This proves that copper species mass transport from the electrolyte bulk toward the cathode surface is the slowest step in electrolyte including various concentrations of the plant extract investigated. The values of activation energies prove that the refining procedure rate was diffusion controlled. Surface morphologies of copper samples were assessed via a scanning electron microscope (SEM) and atomic force microscope (AFM). The chemical composition of the investigated methanolic plant extract was estimated by gas chromatography–mass spectroscopy (GC–MS). Adding elevated methanolic plant extract concentration (1000 ppm) to the refining bath is extremely valuable in improving surface features and appears to have a promising influence. The leveling and grain refining effects were identified. A copper-deposited film with low roughness and high flatness may be obtained. Antimicrobial screening suggests that all-natural product substances demonstrated mild to great action versus the examined organisms. The cathodic current efficiency was decidedly enhanced by improving plant extract concentration in the bath from 200 to 1000 ppm.

Keywords: copper; current efficiency; electrorefining; surface characterization

1. Introduction

Copper is one of the initial metallic elements utilized by human beings. Archeologic shows reveal that individuals in western Asia utilized copper at a minimum of 10,000 an age previously. The community started to develop open stone quarries and manage copper isolated as raw material to deliver missiles, instruments, containers, etc., ahead of six thousand years ago [1]. Copper was dispersed in natural surroundings, and, in the ground, its revenues were the subsequent formulas: sulfide ores, oxide ores, saline minerals, and native copper [2]. Copper and copper composites are employed in different disciplines, comprising building structure, electrical and electrical equipment, engineering machinery devices, transportation apparatus, and other applications, owing to their deterioration-resilient machinable, brilliant deportment, and flexible possessions [3, 4].

Copper minerals cannot be immediately utilized in any manufacture and construction phase procedure, and they should be obtained across extractive metallurgy equipment to isolate sophisticated copper. Overall, the procedure from copper quarrying to processed copper is mentioned as copper fabrication. At present, copper is mostly mined from

highly sulfide ores beyond traditional pyrometallurgical methods. Then, copper is obtained from oxide minerals and a little section of sulfide raw material beyond a hydrometallurgical procedure denoted as solvent-mining electrowinning (SX-EW) manner. The construction stages of various intervals feature substantial discrepancies. The first distinction is the sort of copper minerals from diverse sections, and the second variance is construction dispensation through numerous periods along with extractive metallurgy equipment progress. Owing to these variations, expenditures (such as resource depletion and energy expenditure) and certain ecological contamination troubles also fluctuate [5].

The copper compounds that are a main metal of trade might be potted as follows: elevated electric conduction; elevated heat conduction; easiness of molding, swelling, progressing, and illustration to yield cable, plumbing, and band; low erosion degree of copper once designed for food foundation; outstanding alloying features; elevated aesthetic petition; and little poisonousness to persons. The copper incidence in life in the metal manner managed to its purpose as initial periods both as copper metal and debased with tin like bronze. It was utilized for devices, decorations, jars for food, and currency. Brass alloy remains appealing as decorations. The main use of copper in recent times has been as an electrical performer, and about 50% of the existing demand is for electrical applications. It can be depicted quickly into cables, either single or multifilament, which can be twisted easily and frequently without extreme work strengthening [6].

Electrorefining is a further conventional procedure than electrowinning and like seedlings happens during the world in ranges from 10^3–10^5 tons per year. They are a portion of a longer process to split and regain basic metals as mutually leftover and major minerals. Consequently, the procedure must be constructed to manage an adjustable-feature metal supply and result in an intensity of all the metals present in a form that can be considered further. Electrorefining consistently offers especially high integrity of metal [7].

In an electrorefining procedure, the impure metal is considered an anode, and the contamination should be dropped throughout the metal passage as of the anode toward the cathode in electrolysis. There should be no anode passivation, and the purpose is to acquire a great property, frequently extremely transparent cathode deposit. Where essential, condiments are included in the electrolyte bath to impose the appropriate performance at mutual electrodes. Cl^- ion is a frequent addition to improving the dissolution procedure; organic compounds are utilized to alter the cathode deposit texture. Although organic composites may be obstructed to the extent and decrease the metal integrity, their usage is prevented when feasible [8, 9].

Several plant portion descents, which are an affluent supply for the biochemical composites, have a significant impact. Additionally, they provide a renewable dissolution retardation resource due to their outstanding accessibility and eco-friendliness. Various plant mines can be used as distilling levelers recognized as green distilling seasonings. However, little work has been done on copper electrorefining such as the aromatic and aliphatic amines [10], new diamine additives [11], inorganic salts [12], vitamin C [13, 14], thiourea [15], and almond shell extracts [16].

The utilization of plant extract in copper refining baths has benefited more than its usage of certain organic and inorganic substances since they are nonpoisonous, low-cost, and ecologically approachable [17–19]. Accordingly, this investigation aims to examine the copper electrorefining in the existence of several concentrations of green additives (*Lablab purpureus*, Linseed, Sidr leaves, and Indian costus), as well as the resultant surface morphology investigated via scanning electron microscope (SEM) and surface roughness atomic force microscope (AFM), and also, the cathodic current efficiency will be investigated.

2. Materials and Methods

2.1. Electrorefining Bath Solution. 0.15 M $CuSO_4$ and 1 M H_2SO_4 (98% w/w) are used for copper electrorefining experiments. Demineralized water of computed resistivity > 18 MX/cm. Plant extract preparation with methanol was used as solvent in plant extract preparation. All compounds are provided by BDH Compounds Ltd. All trials were accomplished in 0.15 M $CuSO_4$, 1 M H_2SO_4-free solution, and 0.15 M $CuSO_4$ and 1 M H_2SO_4 containing several concentrations of plant extract (50–1000 ppm).

2.2. Electrode Chemical Composition. Copper was utilized during the trials in sheet form that had the subsequent subject (wt.%), 2.78 cadmium, 0.051 silver, 1.56 lead, 0.629 tin, and 94.98 copper.

2.3. Methanolic Plant Extract Preparation. Linseed (*Linum usitatissimum*), Indian costus (*Saussurea costus*), Sidr leaves (*Ziziphus spina-christi*), and *Dolichos lablab* (Lablab purpures) were bought from the regional shop, rinsed with purified water, and then air dehydrated and individually cut down into face powder utilizing a blinder. Around 50 g of crushed specimens was soddened in 1000 mL methyl alcohol for 14 days (to improve the appropriate combination of methanol along with crushed specimens) at 25°C. The mixtures were then screened to eliminate any contamination and to attain sample excerpts. This standard plant extract was maintained in the freezer, and it is willing to be utilized to manage necessary concentration. The standard solution application was concluded via vaporizing a well-established excess volume to eradicate the solvent and assess the remainder.

2.4. Electrorefining Cell. The electrorefining cell utilized (Figure 1) comprises of quadrangular plexiglass vessel including an improper of $20 \times 5 \times 10$ cm including copper electrodes (10 cm × 5 cm) which match the entire section. Before every trial, the cell was stuffed with 0.15 M $CuSO_4$ and 1.0 M H_2SO_4 solution and the effective cathode height (2 cm) was attuned by shielding the cathode rest via epoxy resin on the immobile portion. The electric circuit comprised a 6 V

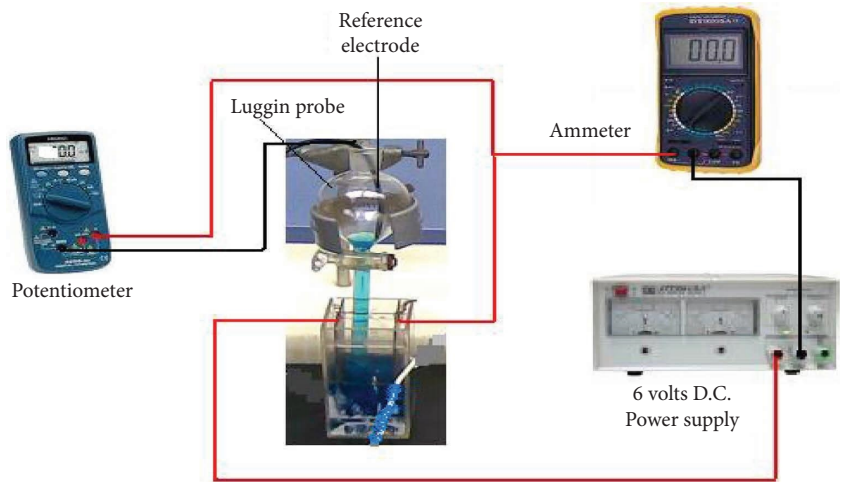


Figure 1: The electrorefining electrical circuit.

DC control supply, a changeable persistence, and a various-scale ampere meter linked in a sequence via cell. A superior impedance voltammetry was attached analogously in conjunction with the cell to determine its voltage. The continual state cathode voltage was assessed versus the reference probe comprised of a tiny copper cable submerged in a goblet of lugging pipe stuffed with 0.15 M $CuSO_4$ and 1.0 M H_2SO_4 plant extract solution. The lugging pipe tip was positioned 0.5–1.0 mm as of the cathode side. Polarization bends, from which the controlling current (I_L) was established, were schemed by growing the employed current piecemeal and calculating the subsequent stable-state cathode voltage. Three minutes were permitted to achieve the constant state voltage. Before each trial, the cathode's other side was padded as well as polystyrene varnish, and the effective surface was smoothed with the excellent abrasive paper piece, washed with trichloroethylene, rinsed with ethanol, and completely washed in purified water. The high was adjusted by putting the container in a thermostat water tub at various temperatures (20°C–50°C) ± 1°C. Limiting current duplicability was approved by running at least three individual trials.

2.5. Characterization

2.5.1. SEM. SEM (JEOL JSM-5300 Imaging Electron Microscope) was conducted on the surface of copper specimens (1 cm × 1 cm) with and without 1000 ppm of four studied plant extracts.

2.5.2. AFM. The copper samples used for atomic force were divided into dimensions (3 × 3) cm and a thickness of approximately ~1 mm. All samples were polished, degreased by acetone, and washed with distilled water. ER process occurred for specimens in electrolytic cells containing 0.15 M $CuSO_4$, 1 M H_2SO_4 free solution, and 0.15 M $CuSO_4$ and 1 M H_2SO_4 containing 1000 ppm four investigated plant extract. The samples were stored in desiccators until they were analyzed.

2.5.3. Fourier Transform-Infrared Spectroscopy (FTIR). For FTIR analyses, A Bruker Tensor 37 FTIR spectrophotometer, device was utilized, and dry plant extract was utilized. The specimens were determined via blending along with potassium bromide. The fields were assessed in the 400–4000 cm^{-1} scale.

2.5.4. Gas Chromatography. GC assessment was conducted utilizing Gas Hewlett Packard HP5890 sequences II with split per split fewer injector and vessel line (28 m, 0.24 mm, and 0.24 mm) combined with phenyl polysil phenylene siloxane. The injection part and indicator heat were 270° and 305°C, correspondingly, and the oven heat was maintained at 85 C for 2 min, rising to 305°C at 22°C/min. Helium was utilized as transporter gas at a persistent stream of 1.0 mL per minute. A capacity of 2 mL was inserted in the breakless method, and the elimination period was 2 min.

2.5.5. Gas Chromatography–Mass Spectrometry (GC–MS) Analysis. The MS (Hewlett-Packard 5889 BMS Engine) with certain ion observation (SIM) was utilized. It was conducted at 70 eV and examined pieces from 50 to 650 m/z.

2.5.6. Component Detection. The procedure conducted for individual component detection for plant isolate was established on chromatographic preservation indicators and by comparison of the acquired MS along with those available in the NIST archive.

3. Result and Discussion

3.1. $CuSO_4$ Concentration Influence on the Limiting Current. Table 1 gives the refining electrolyte ($CuSO_4$) concentration influence on the refining limiting current IL, and it is apparent which limiting current rises while copper sulfate concentration increases. Increasing the $CuSO_4$ concentration in the refining bath leads to reducing the cathodic divergence and enhances the limiting current flat terrain.

Table 1: The influence of various $CuSO_4$ concentrations at the limiting current at 20°C in copper electrorefining.

Conc. $CuSO_4$ (mol/L)	I_L (A)
0.02	0.162
0.05	0.204
0.10	0.282
0.15	0.363
0.20	0.435

These findings were owing to an expansion in the comparative profusion of the uncomplexed Cu^{2+} ions in the electrolyte bath [16].

3.2. Potential-Dynamic Cathodic Polarization Curves. The experiential variations in the cathodic divergence in the presence of methanolic plant extract advocate that it should be acting as a retardation agent, established by the remark that at any assumed over-voltage, the copper deposition current density as of electrolyte comprising methanolic plant extracts is lesser than that originate for the consistent methanolic plant extracts—free bath. This retardation behavior of the methanolic plant extracts in the copper electrorefining response may be owing to the methanolic plant extracts' adsorption in the cathode exterior.

Accordingly, the limiting current diminishes via enhancing methanolic plant extract concentration as indicated in Figure 2, owing to the development of complexes with Cu^{2+} ions. Values of limiting current at various temperatures are presented in Table 2.

Remarkably, Table 3 reveals a diminishing in the limiting current via rising methanolic plant extract concentration and improvement in temperature.

A characteristic current-potential (I–V) plot necessitates to be designed via varying both electrolyte configuration and temperature before electrorefining. An I–V curve (Figure 2) is built through with varying potential and constructed against the cell current. The I–V curve establishes whether the temperature and electrolyte merger is a current plateau. The current plateau is wherever changing in the potential no longer encourages oscillation in the progress current density, suggesting enhanced operation beyond the refining level. As a result of the less diffusion mechanism, a distinct, glutinous coating was delineated on the cathode surface, which outcomes in the interval of the electrochemical response, delivering a current upland on the I–V plot [20, 21].

3.3. Plant Extracts' Characterization

3.3.1. FTIR Spectroscopic Analysis. The heteroatoms subsistence like O, N, and Cl, benzene ring, alongside various functional groupings (hydroxyl, carbonyl, and carbon–carbon double bond) in plant extract might support their particles to adsorb on copper–solution interface to diminish the copper refining. In this research, the FTIR was commissioned to distinguish whether the plant extract includes certain of these efficient groups or not. Table 2 shows some significant functional groups that appear in the extracts.

The resemblance among the absorbance bands performed by FTIR spectra of *Dolichos lablab* (*Lablab purpureus*), Linseed (*Linum usitatissimum*), Sidr leaves (*Ziziphus spina-christi*), and Indian costus (*Saussurea costus*) before and later electrorefining is demonstrated in Figure 3. This absorbance band occasionally appeared, receded, or altered after ER to suggest the development of (Cu-plant extract) composite. Additionally, it is noticed that while the summits were examined for dried-up plant extract beforehand ER is additionally observed for plant extract afterward ER.

3.3.2. Apparently

3.3.2.1. In Dolichos lablab. A powerful hydroxyl band at 3384.6 has changed to 3428.4 cm^{-1}, and C-H extending band at 2927.2 has changed to 2925.68 cm^{-1}. The 1741.1 cm^{-1} absorption band suggests the existence of stretching group C=O, and this band vanished after ER. Bending C=C is changed from 926.8 to 886.1 cm^{-1} and the C-Cl extending band is changed from 551.6 to 501.3 cm^{-1} [22]

3.3.2.2. Linseed (Linum usitatissimum). A powerful and distinct peak of stretching –OH is detected at 3288.72 cm^{-1} before ER and is also monitored at 3587.98 cm^{-1} after ER. C-H extending peak is changed from 2924.63 to 23,916 cm^{-1}. Extending peak of C=O before ER and is as well examined at 1745.21 cm^{-1} after ER. Additionally, the shuddering peak of N-H is situated in 2857.06 cm^{-1}, which shifted to 3199.10 cm^{-1}. The new absorption peaks at 1446.14 cm^{-1} suggest the C=C bending presence that shows at 1446.14 cm^{-1} before ER while at 1457.15 cm^{-1} after ER. The absorption peak of C-O-C extending looked at 1376.33 and altered to 1386.85 cm^{-1}, and stretching C-N has changed from 1246.66 to 1238.42 cm^{-1}. Another absorption peak at 1051.79 cm^{-1} suggests the occurrence of stretching S=O that occurs after ER while 1096.21 cm^{-1} after ER. Stretching C-Cl bands are changed from 667.47, 524.42 cm^{-1} to 716.27 and 609.65 cm^{-1} [23].

3.3.2.3. In Sidr Leaves (Ziziphus spina-christi). The assimilation of –OH stretching peak positioned at 3690.55 changed to 3433.44 cm^{-1}. Moreover, the extending C-H peak is changed from 2513.94 to 2874.58 cm^{-1}. The C=O and C-O bands' stretching incidence changed from 1798.68 to 2514.07 cm^{-1} and 965.21 to 874.37 cm^{-1} correspondingly, owing to electron raincloud compactness change from oxygen atoms to synchronize with copper ions to produce [Cu-plant extract] composite. A stretching peak of C=O before ER is also observed at 1638.96 cm^{-1} before ER while 1798.16 cm^{-1} after ER. The C-Cl enlarging band is changed from 712.03 cm^{-1} to 575.51 cm^{-1} [24].

3.3.2.4. In Indian Costus (Saussurea costus). A wide band at 3691.01 cm^{-1} is ascribed to –OH and/or N-H extending vibrations that changed to 3698.04 cm^{-1}. The C-H stretching peak is changed from 3466.79 to 3097.04 cm^{-1}, bending hydroxyl peak is situated at 1423.88 cm^{-1} and shifted to

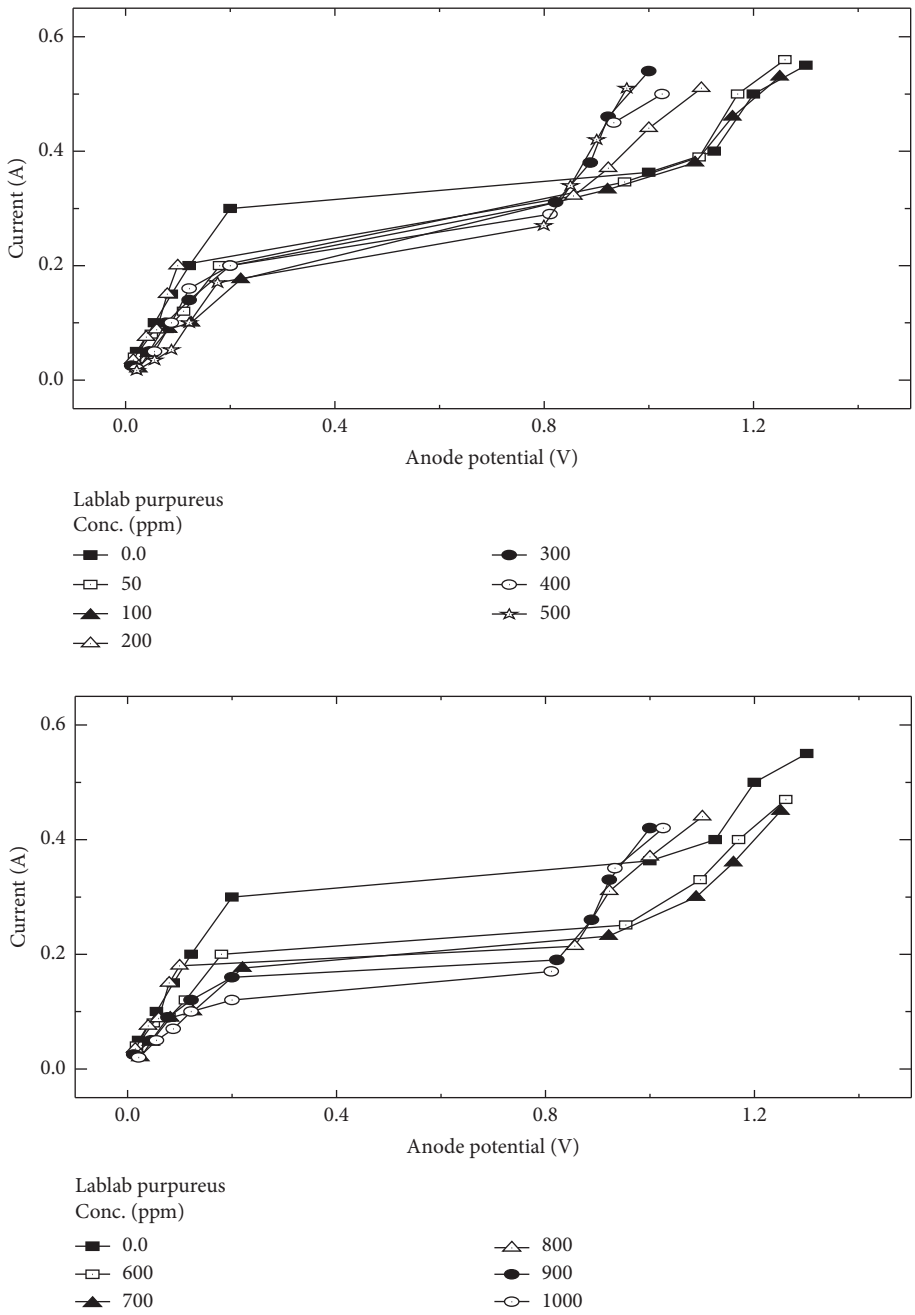


Figure 2: The cathodic polarization curves in copper sulfate-free solution and copper sulfate containing various concentrations of *Dolichos lablab* extract at 20°C.

1796.84 cm^{-1} after ER. The 1640.66 cm^{-1} absorption band is altered 2514.83 cm^{-1}, which could be designated as stretching C=O. C-Cl extending bands are moved from 797.21, 712.22 cm^{-1} to 775.74, 714.35 cm^{-1} [25].

The superficial assessment utilizing FTIR exposes that function groups such as hydroxyl, carboxyl, and carbonyl appear in the organic component of plant isolate that suggested the isolate includes various bioactive particles (great for retardation). The existence and changed spreading peaks of the functional groupings validate the establishment of effective complex Cu^{2+}. Consequently, the FTIR bands show that there is a collaboration among the extract components and the copper substratum that followed in the retardation influence [26].

3.3.3. GC–MS Analysis. The organic composites observed in *Dolichos lablab* (*Lablab purpureus*), Linseed (*Linum usitatissimum*), Sidr leaves (*Ziziphus spina-christi*), and Indian costus (*Saussurea costus*) were discovered via GC–MS analysis. The molecular formula, molecular weight, retention time (RT), and % compositions are described in Table 4.

Table 2: FTIR bands of plant extract from methanol before and later ER.

Dolichos lablab (*Lablab purpureus*)			Linseed (*Linum usitatissimum*)		
Obligation Functional grouping	Before ER Wave number (cm^{-1})	After ER Wave number (cm^{-1})	Obligation Functional grouping	Before ER Wave number (cm^{-1})	After ER Wave number (cm^{-1})
O-H stretching	3384.6	3428.4	O-H stretching	3288.72	3587.98
C-H stretching	2927.2	2925.68	C-H stretching	2924.63	2926.78
C=O stretching	1741.1	—	N-H stretching	2857.06	3199.10
C=C stretching	1636.2	1637.6	C=O stretching	1731.95	1745.21
C-H bending	1411.5 1237.8	1400.1	O-H bending	1650.67	1657.42
C-O stretching	1143.3 1058.3	1143.2	C-O stretching	1614.37	1542.70
C-H stretching	871.2 799.8	—	C=C bending	1446.14	1457.15
C=C bending	926.8	994.7 886.1	C-O-C stretching	1376.33	1386.85
C-Cl stretching	585.8 551.6	501.3	C-H stretching	1320.02	1310.54
			C-N stretching	1246.66	1238.42
			S=O stretching	1051.79	1096.21
			C-Cl stretching	667.47 524.42	716.27 609.65
Sidr leaves (*Ziziphus spina-christi*)			**Indian costus (*Saussurea costus*)**		
O-H stretching	3690.55	3433.4492	O-H stretching	3691.01	3698.04
O-H stretching, N-H stretching	3459.25	2983.0965	C-H stretching	3466.79 2514.62	3097.04 2924.23
C-H stretching, C=O stretching	2513.94 1798.68	2874.5854 2514.0758	C=C stretching	1798.82	2876.58
C=C stretching	1638.96	1798.1634	C=O stretching	1640.66	2514.83
O-H bending	1424.95	1425.9830	O-H bending	1423.88	1796.84
C-H bending	1038.03	1043.3786	C-H bending	1035.47	1434.79
C-O stretching	965.21	874.3719	C-O stretching	962.62	1048.03
C=C bending	874.79	711.2950	C=C bending	874.92	876.37
C-Cl stretching	795.37 712.03	604.6981 575.5151	C-Cl stretching	797.21 712.22	775.74 714.35

3.4. Plant Extract Effect on the Refining Limiting Current. Figure 2 demonstrates polarization curves for cathodic refining of copper in electrolytes comprising various *Dolichos lablab* concentrations at 20°C. The values of limiting current (I_L) were computed by anticipating straight portions of the refining voltage to the crossing of the resultant refining current. I_L values are presented in Table 3. The presence of a distinctive I_L elevation expanding across a broad voltage breadth in the presence of various plant extract concentrations provides that the extract components do not alter the regulated dispersion mechanism of copper refining (mass transportation monitored mechanism) to charge transference mechanism.

If $I_{L(\text{blank})}$ is the blank limiting current and $I_{L(\text{extract})}$ is the limiting current in electrolyte-containing plant extract, then inhibition effectiveness percentage (%IE) may be computed from the subsequent equation:

$$\%\text{IE} = \left(\frac{I_{L(\text{blank})} - I_{L(\text{extract})}}{I_{L(\text{blank})}}\right) \times 100. \quad (1)$$

The cathodic refining rate I_L estimates and proportion %IE for the examined plant extract (50–1000 ppm) and heat limit of 20:50°C with a rise of 10°C are presented in Table 3.

Figure 4 and Table 3 demonstrate that %IE rises as the investigated plant extract concentration rises for *Lablab purpureus* (*Dolichos lablab* extract), Linseed (*Linum usitatissimum*), Sidr leaves (*Ziziphus spina-christi*), and Indian costus (*Saussurea costus*). It is also observed that %IE reduced via temperature raising. The %IE of various plant extracts could be assembled in the sequence:

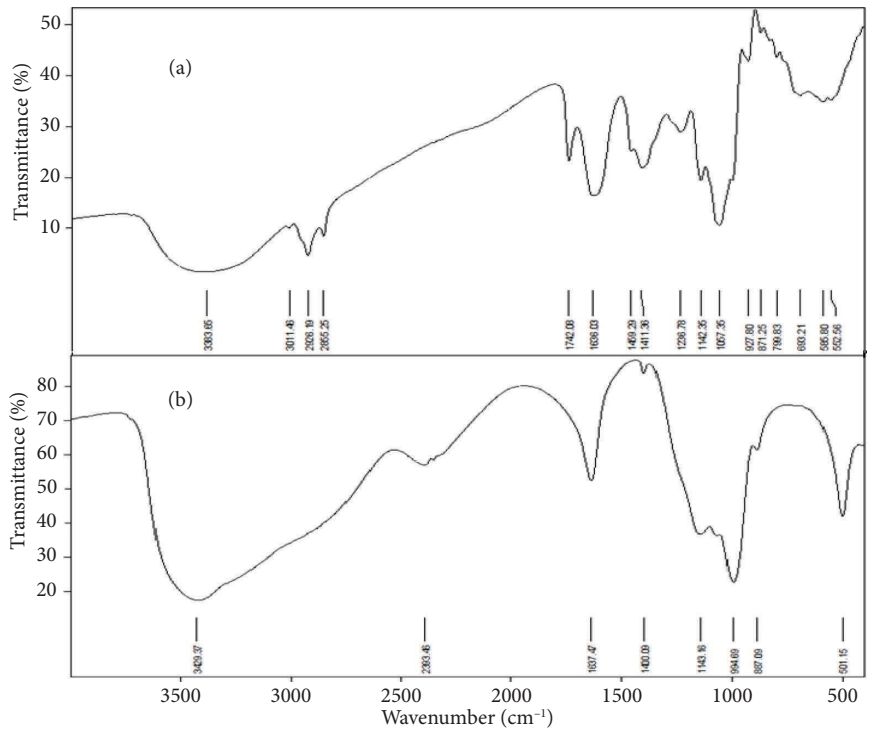
Lablab purpureus (*Dolichos lablab* extract) < Linseed (*Linum usitatissimum*) < Sidr leaves (*Ziziphus spina-christi*) < Indian costus (*Saussurea costus*).

The variance in retardation efficiencies of the investigated plant extracts might be owing to every extract comprising a considerable number of compounds (recognized using GC–MS their comparative proportions are described in Table 4) that are existing in diverse quantities contingent on the extracted kind.

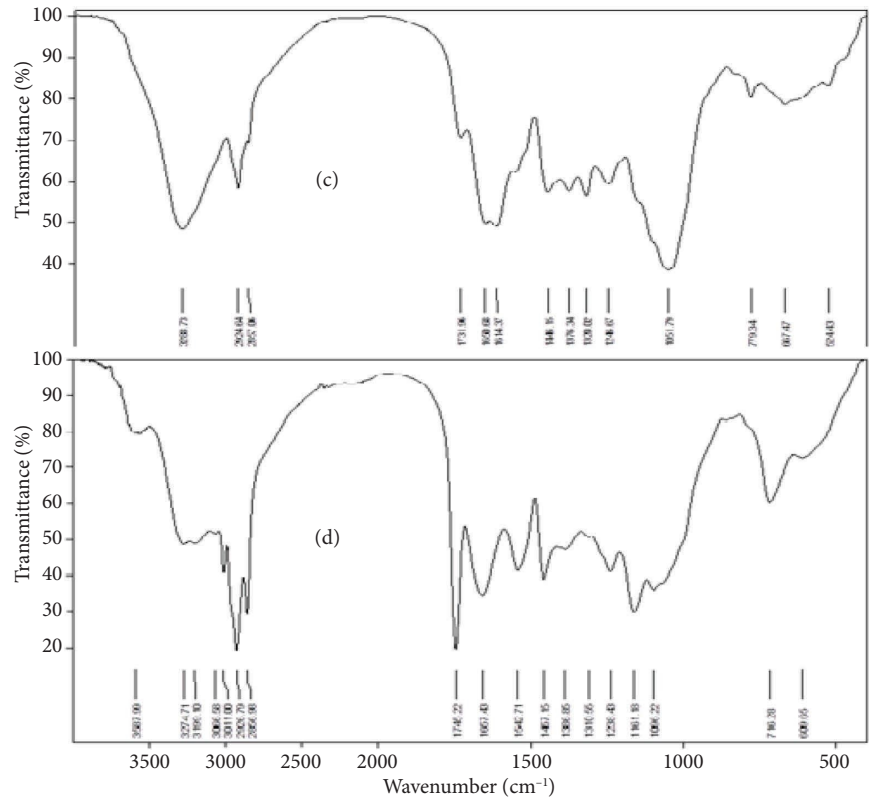
Table 3: Limiting current (A) and % inhibition effectiveness % IE values for the four investigated methanolic plant extracts as a function of concentration and temperature.

Plant extract	Temp	20°C		30°C		40°C		50°C	
	Conc. (ppm)	IL	% IE	IL	% IE	IL	% IE	IL	% IE
Dolichos lablab (*Lablab purpureus*)	0.0	**0.363**		**0.452**		**0.552**		**0.642**	
	50	0.346	4.68	0.432	4.42	0.534	3.26	0.623	2.96
	100	0.333	8.26	0.421	6.85	0.515	6.70	0.607	5.45
	200	0.322	11.29	0.403	10.84	0.500	9.42	0.585	8.88
	300	0.311	14.32	0.388	14.15	0.482	12.68	0.562	12.46
	400	0.290	20.11	0.365	19.25	0.465	15.76	0.543	15.42
	500	0.270	25.61	0.346	23.45	0.443	19.75	0.524	18.38
	600	0.251	31.02	0.324	28.32	0.422	23.55	0.506	21.18
	700	0.232	36.09	0.300	33.63	0.405	26.63	0.490	23.67
	800	0.214	41.04	0.285	36.94	0.382	30.80	0.472	26.48
	900	0.190	47.65	0.262	42.03	0.364	34.06	0.455	29.13
	1000	0.170	53.17	0.244	46.02	0.334	39.49	0.437	31.93
Linseed (*Linum usitatissimum*)	0.0	**0.363**		**0.452**		**0.552**		**0.642**	
	50	0.333	8.26	0.418	7.52	0.515	6.70	0.605	5.76
	100	0.321	11.57	0.400	11.50	0.497	9.96	0.581	9.50
	200	0.300	17.35	0.383	15.26	0.480	13.04	0.563	12.30
	300	0.282	22.31	0.365	19.24	0.464	15.94	0.546	14.95
	400	0.265	26.99	0.352	22.12	0.444	19.56	0.527	17.91
	500	0.247	31.96	0.334	26.11	0.423	23.37	0.508	20.87
	600	0.224	38.29	0.315	30.31	0.407	26.27	0.486	24.30
	700	0.203	44.08	0.292	35.40	0.386	30.07	0.466	27.41
	800	0.181	50.14	0.275	39.16	0.365	33.87	0.444	30.84
	900	0.164	54.82	0.255	43.58	0.347	37.14	0.425	33.80
	1000	0.144	60.33	0.233	48.45	0.322	41.67	0.407	36.60
Sidr leaves (*Ziziphus spina-christi*)	0	**0.363**		**0.452**		**0.552**		**0.642**	
	50	0.321	11.57	0.408	9.73	0.508	7.97	0.598	6.85
	100	0.305	15.98	0.388	14.16	0.489	11.41	0.577	10.12
	200	0.290	20.11	0.369	18.36	0.468	15.22	0.556	13.39
	300	0.271	25.34	0.348	23.00	0.447	19.02	0.533	16.97
	400	0.255	29.75	0.329	27.21	0.432	21.74	0.514	19.94
	500	0.240	33.88	0.308	31.85	0.420	23.91	0.500	22.12
	600	0.220	39.39	0.288	36.28	0.400	27.54	0.482	24.92
	700	0.200	44.90	0.267	40.93	0.382	30.79	0.460	28.34
	800	0.170	53.17	0.247	45.35	0.363	34.24	0.438	31.77
	900	0.150	58.68	0.231	48.89	0.340	38.41	0.416	35.20
	1000	0.123	66.11	0.216	52.21	0.317	42.57	0.398	38.00
Indian costus (*Saussurea costus*)	0	**0.363**		**0.452**		**0.552**		**0.642**	
	50	0.300	17.35	0.400	11.50	0.488	11.59	0.586	8.72
	100	0.283	22.04	0.380	15.92	0.463	16.12	0.564	12.15
	200	0.264	27.27	0.360	20.35	0.444	19.56	0.546	14.95
	300	0.245	32.50	0.340	24.77	0.425	23.00	0.524	18.38
	400	0.222	38.84	0.322	28.76	0.407	26.27	0.507	21.02
	500	0.205	43.52	0.304	32.74	0.393	28.80	0.487	24.14
	600	0.184	49.31	0.285	36.94	0.375	32.06	0.465	27.57
	700	0.167	53.99	0.262	42.03	0.355	35.69	0.444	30.84
	800	0.144	60.33	0.244	46.02	0.336	39.13	0.425	33.80
	900	0.120	66.94	0.222	50.88	0.318	42.39	0.407	36.60
	1000	0.092	74.65	0.200	55.75	0.292	47.10	0.380	40.81

The beneficial influence of these compounds was a hindrance to the refining procedure for copper in $CuSO_4$ electrolyte. It may be suggested that the efficient chemical compounds in this extract include functional groups that may be utilized as adsorption sites because they include oxygen or nitrogen and halogen atoms. The adsorption spots electron density, and subsequently, the extracted power is the adsorption performance on the copper surface relying on its chemical composition, its molecular dimension, and the charge dispersal around the full retardation molecule. This suggests the perceived variations in the %IE among the numerous extracts and results in the sequence:



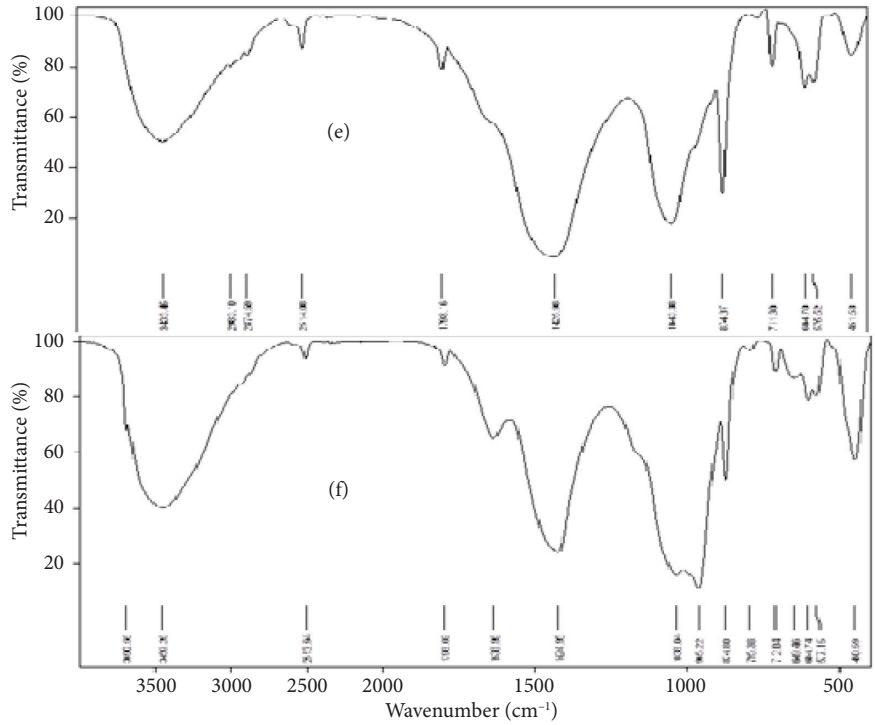
Dolichos lablab *(Lablab purpureus)*



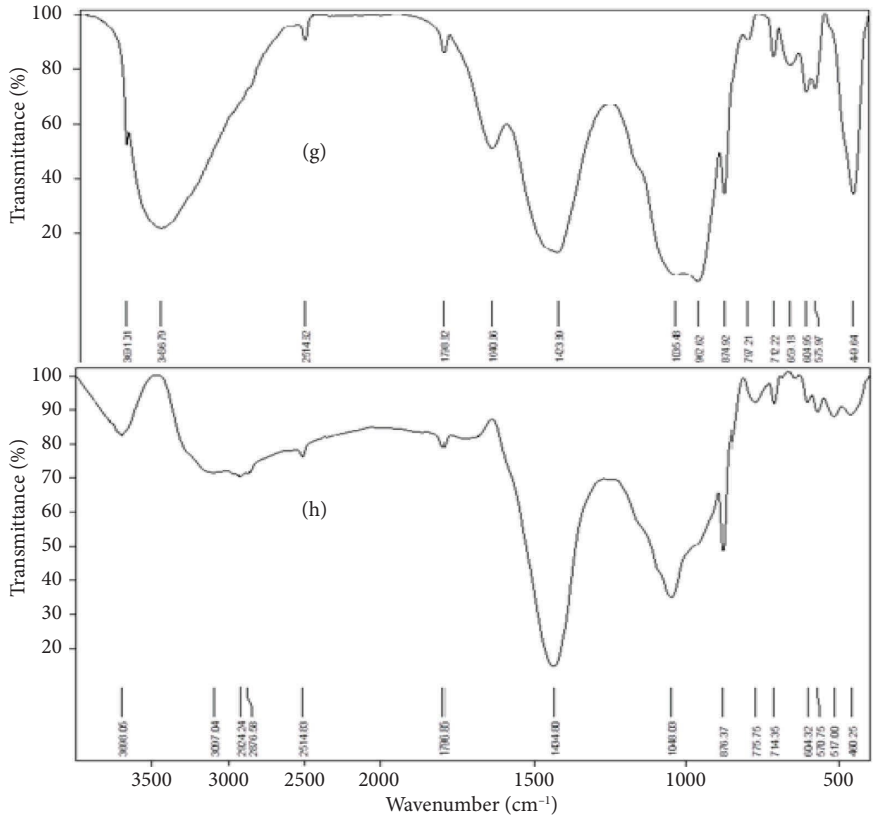
Linseed *(Linum usitatissimum)*

(a)

Figure 3: Continued.



Sidr leaves *(Ziziphus spina-christi)*



Indian costus *(Saussurea costus)*

(b)

Figure 3: FTIR bands for plant extract from methanol (a, c, e , g) before ER and (b, d, f, h) after ER.

Table 4: Some of the chemical components identified in plant extract by GC–MS.

No.	Identified compound	Molecular formula	Molecular weight	RT	% compositions
Dolichos lablab (*Lablab purpureus*)					
1	Docosahexaenoic acid, 1,2,3-propanetriyl ester	$C_{69}H_{98}O_6$	1022	5.37	4.89
2	Hexadecanoic acid, methyl ester	$C_{17}H_{34}O_2$	270.1	20.94	5.10
3	Oleic acid	$C_{18}H_{34}O_2$	282.2	21.66	5.36
4	7,10-Octadecadienoic acid, methyl ester	$C_{19}H_{34}O_2$	294.3	24.09	11.13
5	Linoleic acid chloride	$C_{18}H_{31}ClO$	298.1	24.20	6.65
6	α-Glyceryl linoleate	$C_{21}H_{36}O_4$	352.1	24.98	28.50
7	Giganteumgenin N	$C_{30}H_{50}O_6$	506.2	28.07	4.07
8	Linoleic acid	$C_{18}H_{32}O_2$	280.2	31.05	21.49
9	Diisooctyl phthalate	$C_{24}H_{38}O_4$	390.3	31.54	12.80
Linseed (*Linum usitatissimum*)					
1	Tricyclo[4.1.0.0(2,7)]hept-3-ene	C_7H_8	92.2	4.26	75.84
2	1,4-Dimethyl benzene	C_8H_{10}	106.1	6.76	2.59
3	4-Methyl-2-pentanol	$C_6H_{14}O$	130.1	5.23	8.76
4	Oleic acid	$C_{18}H_{34}O_2$	282.2	4.34	0.85
5	Chloroacetic acid, octyl ester	$C_{10}H_{19}ClO_2$	207.3	4.54	5.12
6	7-Methyl-tetracyclo [4.1.0.0(2,4).0(3,5)] heptane	C_8H_{10}	106.1	6.55	2.00
7	1,4-Diphenylbut-3-ene-2-ol	$C_{16}H_{16}O$	224.2	4.93	0.58
8	1,4-Diphenyl-1,2-dihydrophthalazine	$C_{20}H_{16}N_2$	284.2	9.41	0.79
9	Methoxyacetic acid, cyclohexyl ester	$C_9H_{16}O_3$	172.2	5.66	0.69
10	12,15-Octadecadienoic acid	$C_{18}H_{32}O_2$	280.2	7.63	0.78
11	Cyclohexene, 1-(2-nitro-2-propenyl)-	$C_9H_{13}NO_2$	167	4.47	0.57
12	1-(5-Chloro-2-methoxyphenyl)-1H-pyrrole	$C_{11}H_{10}NOCl$	207	17.15	0.43
Sidr leaves (*Ziziphus spina-christi*)					
1	Phenol, 2,5-bis(1,1-dimethyl ethyl)-	$C_{14}H_{22}O$	206	37.35	40.00
2	2-Methyl-decane	$C_{11}H_{24}$	156	21.11	18.98
3	Disulfide, di-tert-dodecyl 9,12,15-octadecatrienoic acid	$C_{24}H_{50}S_2$	402	26.13	15.61
4	Nonadecane	$C_{19}H_{40}$	268	23.84	8.6
5	1-Dodecene	$C_{12}H_{24}$	168	28.60	2.89
6	Aspidospermidin-17-ol, 1-acetyl-16-methoxy-	$C_{22}H_{30}N_2O_3$	370	30.25	3.5
7	1-Fluoro-dodecane	$C_{12}H_{25}F$	188	24.48	2.46
8	2,6-Di-t-butyl-4-methylene-2,5-cyclohexadiene-1-one	$C_{15}H_{22}O$	218	20.93	2.22
9	6-Epi-shyobunol phenol	$C_{15}H_{26}O$	222	33.54	1.88
10	18-Methyl-nonadecanol, trimethylsilyl ether	$C_{23}H_{50}Osi$	370	23.45	1.32
11	Tetradecamethylcycloheptasiloxane	$C_{14}H_{42}O_7Si_7$	519	21.35	1.18
12	1-Monolinoleoylglycerol trimethylsilyl ether	$C_{27}H_{54}O_4Si_2$	501	32.76	1.22
Indian costus (*Saussurea costus*)					
1	Hexadecanoic acid, methyl ester	$C_{17}H_{34}O_2$	270.45	22.69	13.8 4
2	11-Octadecenoic acid, methyl ester	$C_{19}H_{36}O_2$	296.5	26.09	30.0 7
3	9-Octadecenoic acid, 12-hydroxy-, methyl ester, [R-(Z)]-	$C_{19}H_{36}O_3$	312.48	29.57	25.87
4	9,12-Octadecadienoic acid, methyl ester	$C_{19}H_{34}O_2$	294.5	25.94	12.55
5	Linoelaidic acid	$C_{18}H_{32}O_2$	280.4	25.26	1.28
6	Methyl stearate	$C_{19}H_{38}O_2$	298.50	26.57	7.97
7	2-Methyl-Z, Z-3,13-octadecadienol	$C_{19}H_{36}O$	280.5	32.55	1.51
8	9-Octadecenoic acid (Z)-, methyl ester	$C_{19}H_{36}O_2$	296.48	26.17	1.86
9	9,12-Octadecadienoi c acid (Z, Z)-, methyl ester	$C_{19}H_{34}O_2$	294.47	26.89	1.66
10	9,17-Octadecadienal, (Z)-	$C_{18}H_{32}O$	264.4	36.10	1.45
11	9,12-Octadecadien-1-ol, (Z, Z)-	$C_{18}H_{34}O$	266.5	36.13	0.98
12	7-Octadecenoic acid, methyl ester	$C_{19}H_{36}O_2$	296.5	29.66	0.85

Lablab purpureus (*Dolichos lablab* extract) < Linseed (*Linum usitatissimum*) < Sidr leaves (*Ziziphus spina-christi*) < Indian costus (*Saussurea costus*).

It was noticed as contrived in Figure 4 that the inhibition efficiency improved as the concentration enhanced, becoming as high as 74.65%. Phytochemical screening of the Indian costus (*Saussurea costus*) extract suggested the existence of sesquiterpenes, triterpenes, flavonoids, and lignans [27]. These chemical components may be accountable for the great retardation effectiveness of the Indian costus (*Saussurea costus*) as these components when adsorbed to the metal surface become barricades to charge transfers among the electrolyte bath and the metal; moreover, the presence of conjugate dual bonds in these compounds is recognized from GC–MS (Table 4) and FTIR (Table 2). Furthermore, the high costus (*Saussurea costus*) hindrance execution suggests strong bonding of the efficient composites and copper surface as a result of heteroatoms (O,

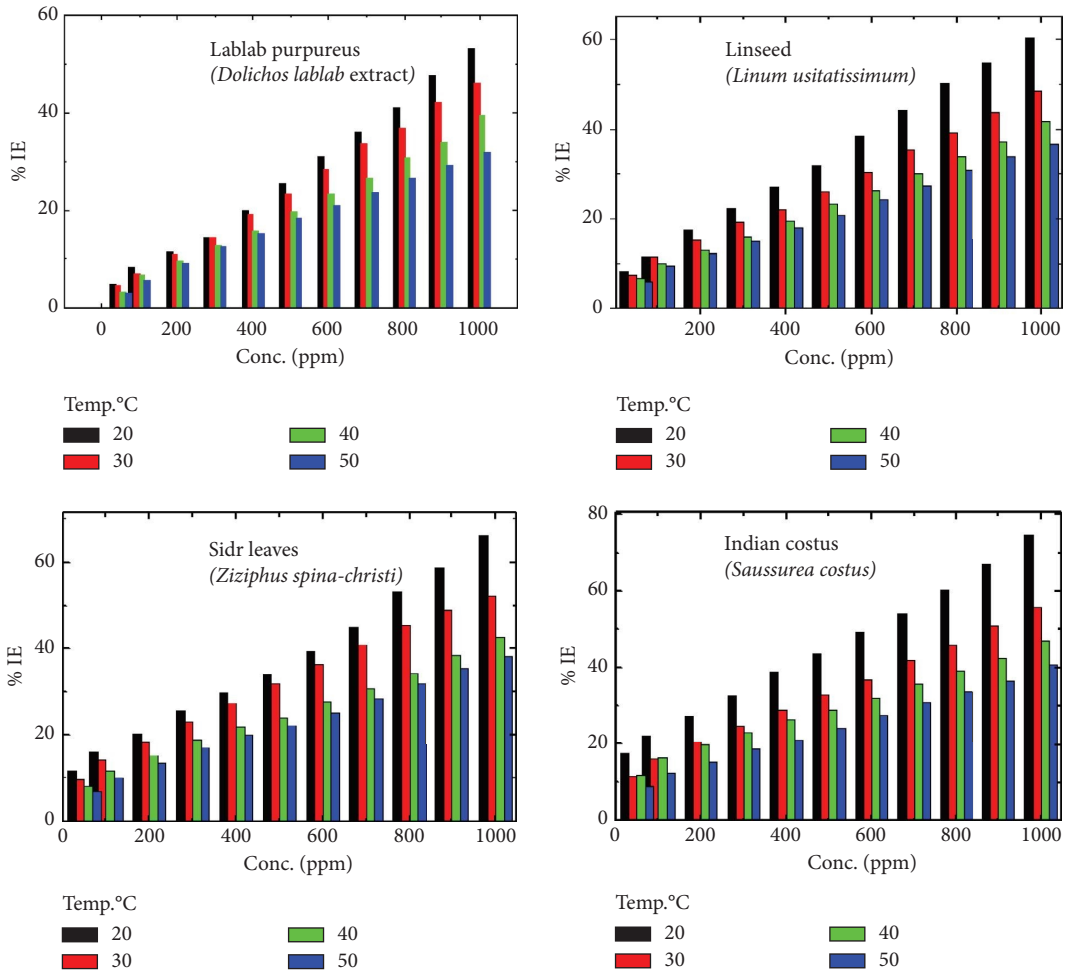


Figure 4: Inhibition effectiveness percentage (% IE) as a function of methanolic plant extract concentration curves for copper in acidified copper sulfate solution.

N), lone pairs of electrons, and π-orbital preventing the active locations and consequently diminishing the deposition rate. Consequently, the connection among retardation molecules and $CuSO_4$ happens across the contribution of the oxygen atoms of electrons (OH group) appear in the labeled composites (Table 4) of the costus extract (*Saussurea costus*) and vacant copper d-orbital. Additionally, *Saussurea costus* molecules may attract on the copper surface based on subscriber–acceptor communication among π-electrons in benzene rings and copper vacant d-orbital [28].

Additional examination of Figure 4 and Table 3 establishes that hindrance effectiveness values increase through increasing concentration and however diminish along with improving temperature. Reduction in %IE by rising temperature implies that the plant extract molecules were adsorbed on the copper surface in a physical approach.

The retardation influence of Sidr leaves (*Ziziphus spina-christi*) extracts may be ascribed to the adsorption of effectual ingredients containing tyrosol, hydroxytyrosol, *p*-hydroxybenzoic acid, vanillic acid, caffeic acid, ferulic acid, tannic acid, and cinnamic acid. The active components of these extracts are demonstrated in Table 4.

FTIR demonstrates that Sidr leaves (*Ziziphus spina-christi*) include oxygen and nitrogen atoms in functional groupings (OH, C=O, C-O, C-N, N-H, C=C) and benzene rings, which meets the overall importance of characteristic retardation molecules. Additionally, owing to polar atoms lone-pair electrons in *Ziziphus spina-christi* elements may merge with recently produced Cu^{2+} ions on copper outward producing [Cu-plant extract] complex. These complexes may get engrossed in the copper–liquid interface via van der Waals interaction [26, 27].

The inhibiting effect of Linseed (*Linum usitatissimum*) extracts can be ascribed to the adsorption of efficient components containing (linolenic acid, palmitic acid, oleic acid, and high content of di- and tri-unsaturated esters). The successful ingredients of these extracts are displayed in Table 4. These composites were thought to be excellent applicants for deposition restraint owing to the existence of heteroatoms (O), several functional groups –(OH), electron providing $-(CH_3)$ group π-electron, and benzene ring as adsorption clusters [29].

The linseed structure includes greater density of (C = C and OH) groups than other additives, which are required with copper ions. The metal deposition occurs with superior

effectiveness although nothing of the metal contamination can move from the anode to the cathode. There should be no anode passivation, and the purpose is to acquire a great excellent, frequently extremely glowing cathode deposit. Wherever essential, additives are included in the electrolyte to impose the proper performance at mutual electrodes. Wherever essential, organic compounds are used to alter the cathode deposit. Because organic composites may be obstructed to some extent and diminish metal purity, their use is averted when feasible.

The retardation influence of *Lablab purpureus* (*Dolichos lablab* extract) is ascribed to the adsorption of effective components containing steroids, sugar, essential oils, alcohols, phenols, saponins, alkaloids, tannins, anthnanoids, flavonoids, pigments, coumarins, terpenoids, and glycosides. The compound structures shown in Table 4 expose that there is a profusion of O-H, C=O, C-O, $-CH_3$, and benzene rings. This certainty has been established among the analogous peaks in the FTIR (Figure 3). Consequently, it is sufficient to assert that extracting effectiveness versus copper is appropriate to the profitable chemical component's adsorption [27, 30].

It might be assumed that the synergetic collaboration of the main elements in the four examined plant extracts along with other chemical components adds to the considerable extract's retardation property.

- The prevalence of an enormous number of hydroxyl groups and carboxylic acid of the four considered methanolic plant extracts may interact with water via the hydrogen bonds that would require higher energy to break, which leads to a reduction in the copper ions' mobility and diffusivity, with a consequential diminution in the electrorefining rate.
- Rising solution viscosity in the existence of these extracts diminishes Cu^{2+} ion's electric conductivity; this led to an impediment in solution flow through the cathodic surface thus limiting current value.
- In an aqueous acidic solution, the four investigated methanolic plant extract components might be protonated and exist in a cation manner. Thus, it is simpler for the protonated species to consider the copper surface negatively charged owing to the electrostatic attraction since sulfate is adsorbed on the copper surface. The protonated component species might adsorb via electrostatic collaboration among the positively charged particles and negatively charged cathode surface (physiosorption). Once cations (protonated particles) are adsorbed on copper–electrolyte interface, a coordination bond might be created by subjective electron conversion from particles to the copper surface [31, 32].

3.5. Influence of Temperature. The temperature impact on the cathodic copper refining rate in electrolyte-free solution and electrolyte-containing plant extract was recognized in the temperature range (20°C–50°C). It was revealed that the cathodic refining rate increased with an improvement in temperature for the numerous methanolic plant extract concentrations. The temperature growth led to magnifying the diffusion constant, D, of the rate-determining particle estimates. The temperature is D dependent in proportion to equivalence:

$$D = D_o \exp^{-(\mathrm{Qd}/RT)}, \tag{2}$$

where D_o is the pre-exponential constant, Qd is diffusion activation energy ($kJ{\cdot}mol^{-1}$), T is the temperature in (kelvin, K), and R is the gas constant ($8.314\,JK^{-1}{\cdot}mol^{-1}$).

The E_a estimates that have been multiplied via slopes of the Arrhenius curves [30, 32]:

$$\log I = \frac{\mathrm{Log}\, A - E_a}{2.303\mathrm{R\,T}}. \tag{3}$$

A is a pre-exponential constant. Figure 5 signifies ln I and 1/T plot for the blank electrolyte and electrolyte containing numerous methanolic plant extract concentrations and demonstrates prompt curves and the E_a value has been calculated from Arrhenius plots slopes which are displayed in Table 5. It is revealed that E_a implications in plant extract-free electrolyte and electrolyte comprising plant extract are $< 40\,kJ{\cdot}mol^{-1}$, suggesting that the cathodic refining process is monitored via diffusion [33]. It is observed that as methanolic plant extract concentration increases, E_a increases. The higher values of E_a are good evidence of the strong retardation, behavior of four investigated methanolic plant extracts for the electrorefining processes for Cu metal.

The pre-exponential aspect (A), for the dissimilar reaction, is associated with the active center's number. The adsorbed retardation particles prevent a vital component of the effective positions, i.e., those with the smallest E_a value, on the metal–electrolyte interface. Alternatively, these active clusters have various forces if an enthusiastic surface discrepancy is understood. There are two opportunities: in the first example (E_a, additives > E_a, free electrolyte) that examined in the four investigated plant extracts, where the A values of in electrolyte-containing plant extract are larger than that of copper sulfate—plant extract-free solution (Table 5). The methanolic plant extract particles are adsorbed on the highly active adsorption spots (having the smallest energy), and the deposition procedure occurs primarily on the effective spots of greater energy. In the second example (E_a, additives < E_a, free solution), the A values in the existence of additives are smaller than in free electrolytes. That is, a minor number of additional effective spots persist uncovered that participate in the refining procedure.

3.6. Activated Parameters. The activation parameters of the studied system ($\Delta H^{\#}$, $\Delta S^{\#}$, and $\Delta G^{\#}$) were estimated from the following equations:

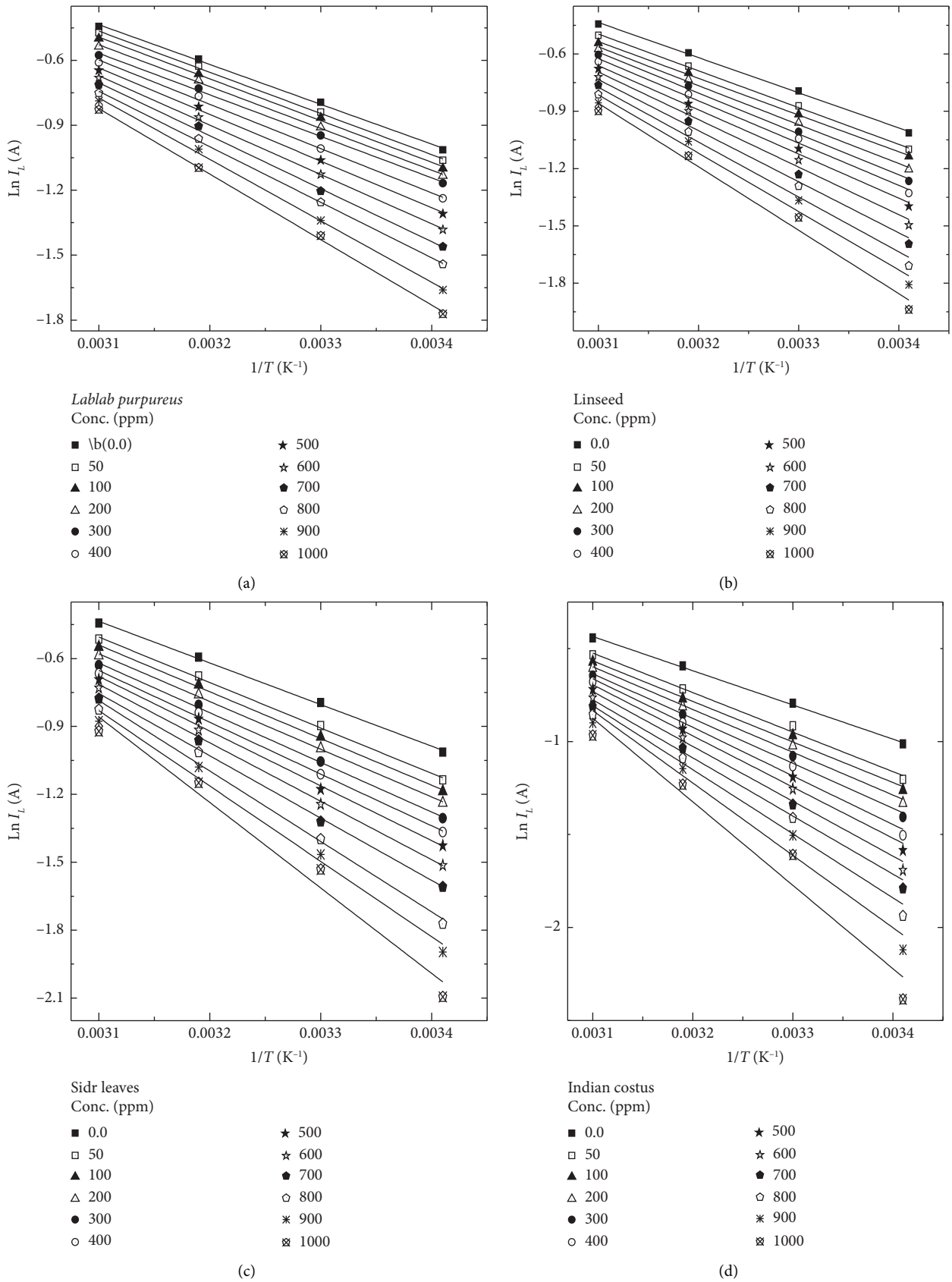


Figure 5: Arrhenius plot of the copper refining in the presence of various concentrations of (a) *Lablab purpureus*, (b) linseed, (c) Sidr leaves, and (d) Indian costus.

Table 5: Activated energy and activated factors for copper refining in acidified copper sulfate.

Compound	*Lablab purpureus* (*Dolichos lablab* extract)								
Conc. (ppm)	E_a (kJ·mol^{-1})	A	R^2	SD	ΔH^* (kJ·mol^{-1})	$-\Delta S^*$ (J·mol^{-1}·K^{-1})	ΔG^* (kJ·mol^{-1})	R^2	SD
0.0	15.30	192.48	0.98	0.063	12.70	209.76	74.16	0.98	0.064
50	15.82	228.15	0.98	0.067	13.23	208.41	74.29	0.98	0.071
100	15.95	239.84	0.98	0.067	13.43	208.00	74.37	0.98	0.071
200	16.03	235.10	0.98	0.067	13.47	208.18	74.47	0.98	0.071
300	16.07	217.02	0.98	0.067	13.35	209.01	74.59	0.98	0.071
400	17.01	311.06	0.98	0.067	14.42	205.76	74.71	0.98	0.071
500	17.91	419.89	0.98	0.067	15.31	203.35	74.89	0.98	0.071
600	18.95	595.85	0.98	0.067	16.36	200.42	75.08	0.98	0.071
700	20.36	972.62	0.98	0.067	17.76	196.33	75.28	0.98	0.071
800	21.33	1352.9	0.98	0.067	18.74	193.63	75.47	0.98	0.071
900	23.61	3071.7	0.97	0.071	21.02	186.84	75.76	0.97	0.075
1000	25.17	5218.7	0.96	0.073	22.57	182.42	76.02	0.97	0.075
	Linseed (*Linum usitatissimum*)								
0.0	15.30	192.48	0.98	0.063	12.70	209.76	74.16	0.98	0.064
50	16.00	237.46	0.98	0.067	13.41	208.09	74.36	0.98	0.071
100	16.22	225.88	0.98	0.067	13.39	208.49	74.48	0.98	0.071
200	16.94	314.19	0.98	0.067	14.34	205.77	74.63	0.98	0.071
300	17.81	423.68	0.98	0.067	15.21	203.31	74.78	0.98	0.071
400	18.37	507.75	0.98	0.067	15.79	201.78	74.91	0.98	0.071
500	19.23	665.14	0.98	0.067	16.64	199.48	75.08	0.98	0.071
600	20.70	1124.39	0.98	0.067	18.11	195.20	75.30	0.98	0.071
700	22.24	1919.84	0.98	0.067	19.65	190.74	75.53	0.98	0.071
800	23.89	3411.81	0.98	0.067	21.30	185.98	75.79	0.98	0.071
900	25.42	5767.53	0.98	0.067	22.83	181.56	76.03	0.97	0.075
1000	27.62	12,581.7	0.96	0.073	25.03	175.11	76.33	0.96	0.076
	Sidr leaves (*Ziziphus spina-christi*)								
0.0	15.30	192.48	0.98	0.063	12.70	209.76	74.16	0.98	0.064
50	16.70	304.90	0.98	0.067	14.11	206.02	74.48	0.98	0.071
100	17.17	350.72	0.98	0.067	14.57	204.87	74.57	0.98	0.071
200	17.53	383.75	0.98	0.067	14.94	204.06	74.73	0.98	0.071
300	18.25	482.99	0.98	0.067	15.65	202.17	74.88	0.98	0.071
400	19.03	626.40	0.98	0.067	16.43	200.03	75.03	0.98	0.071
500	20.12	915.98	0.98	0.067	17.53	196.86	75.21	0.98	0.071
600	21.48	1465.6	0.98	0.067	18.89	192.94	75.42	0.98	0.071
700	22.90	2392.3	0.98	0.067	20.31	188.89	75.65	0.98	0.071
800	25.89	7044.5	0.98	0.067	23.30	179.86	76.00	0.98	0.071
900	27.69	13,226	0.98	0.067	25.09	174.68	76.27	0.97	0.075
1000	31.41	51,534	0.96	0.073	28.82	163.36	76.68	0.96	0.076
	Indian costus (*Saussurea costus*)								
0.0	15.30	192.48	0.98	0.063	12.70	209.76	74.16	0.98	0.064
50	17.67	428.37	0.98	0.067	15.08	203.16	74.60	0.98	0.071
100	18.14	490.78	0.98	0.067	15.54	202.08	74.75	0.98	0.071
200	19.12	685.39	0.98	0.067	16.53	199.27	74.92	0.98	0.071
300	20.05	934.49	0.98	0.067	17.45	196.73	75.09	0.98	0.071
400	21.73	1685.80	0.98	0.067	19.13	191.75	75.31	0.98	0.071
500	22.87	2514.92	0.98	0.067	20.28	188.48	75.50	0.98	0.071
600	24.53	4491.76	0.98	0.067	21.94	183.65	75.75	0.98	0.071
700	25.98	7405.66	0.98	0.067	23.39	179.50	75.98	0.98	0.071
800	28.65	18,033.7	0.98	0.067	26.06	171.52	76.31	0.98	0.071
900	32.35	59,874.1	0.98	0.067	29.76	160.30	76.72	0.97	0.075
1000	37.31	455,886	0.96	0.073	34.71	145.25	77.26	0.96	0.076

$$I_L = \frac{RT}{Nh}\exp\left(\frac{\Delta S^{\#}}{R}\right) \quad \exp\left(\frac{-\Delta H^{\#}}{RT}\right),$$
$$\Delta G^{\#} = \Delta H^{\#} - T\Delta S^{\#}, \tag{4}$$

where h is the Plank, s is constant, N is Avogadro's number, $\Delta H^{\#}$ is the enthalpy of activation, $\Delta S^{\#}$ is the entropy of activation, and $\Delta G^{\#}$ is the free energy of activation. The activation parameter statistics characterized in Table 5 suggest that:

1. The positive signs of $\Delta H^{\#}$ reflect that copper electrorefining is endothermic (Figure 6).
2. The greater the number of configurations of the microscopic particles (atoms, ions, molecules) among the energy levels in a particular state of a system, the greater the entropy of the system. The $\Delta S^{\#}$ entropy negative values suggest that the activated compound is more ordered than reactant species which reflects the methanolic plant extract particles are adsorbed on the copper surface (Figure 6).
3. The $\Delta G^{\#}$ values in an electrolyte comprising plant extract were further positive than that for blank electrolyte for electrorefining processes exposing that in the existence of plant extract, the activated compound turns into a less stable being as associated with its absence [34, 35].

3.7. Adsorption Isotherm. To obtain more evidence about the adsorption mode of methanolic plant extract on the copper surface, it is normally the same opinion that the adsorption isotherm for the metal surface is a central responsibility of the retardation materials mechanism accomplishment destructive acid media. Four adsorption categories might occur in the hindrance incidents relating to organic compounds at the metal–liquid boundary specifically:

a. Charged particles and the charged meta electrostatic attraction.
b. Lone pair of electrons in the particles interacted through the metal.
c. Electrons–metal interface.
d. A combination of the above [36].

Chemisorption includes distribution or charge transport from the retardation particle toward the metal façade that sketch coordination linkage electron transport is distinguishing in conversion metals having vacant lesser energy electron orbital.

Regarding retardation materials, electron transport may be illustrated via molecules having responsibly heavily constrained electrons. This circumstance may happen due to the occurrence of several bonds or a Π character of aromatic rings [36].

The retardation effectiveness of organic substances homologous series, deviate only in the hetero atom, is typically in the chronological series:

$$\mathrm{P} > \mathrm{Se} > \mathrm{S} > \mathrm{N} > \mathrm{O}. \tag{5}$$

The electrochemical procedures above the metal interface are likely to be intimate to the retardation materials adsorption that is established to differ on the retardation materials structure [37].

The investigational statistics have been examined with three adsorption isotherms (Langmuir, Flory–Huggins, and kinetic–thermodynamic type). The adsorption isotherm correlation of Langmuir, Flory–Huggins, and kinetic–thermodynamic model is characterized by equivalences as follows [37]:

$$\frac{C}{\theta} = \frac{1}{K} + C, \tag{6}$$

$$\mathrm{Log}\frac{\theta}{\mathrm{C}} = \log xK + x\log(1-\theta), \tag{7}$$

$$\log\left(\frac{\theta}{1-\theta}\right) = \log K' + y\log C, \tag{8}$$

where θ is the surface coverage, $\theta = ((I_{L(\mathrm{blank})} - I_{L(\mathrm{extract})})/I_{L(\mathrm{blank})})$; K is the equilibrium constant; and C is the bulk solution concentration. x is the water molecule number changed by one retardation molecule. y is the retardation molecule number dominating one effective site. y values are larger than one that indicates the multilayer realization of the retardation on the metal surface; however, y values are fewer than one suggesting that the inhibitor will dominate further than one effective site. K' is a constant affiliated with the adsorption process binding constant K by the subsequent correlation:

$$\mathrm{K} = K'^{(1/Y)}, \tag{9}$$

where $1/y$ signifies the active site number on the surface dominated by one inhibitor particle [33].

The representative Langmuir adsorption curve (Figure 7(a)) was acquired at 20°C with numerous concentrations of plant extract that is represented in Figure 7(a). The straight curve has a slope value equal to 0.93, 1.12, 1.14, and 1.12 (Table 6). These results could also indicate that four studied methanolic plant extracts dominated one adsorption site on the copper surface [38]. Langmuir isotherm believes consistent occupation on the surface for adsorption to occur and no interaction among adsorbed particles. The values of R^2 obtained in the Langmuir isotherm are closest to unity, suggesting that the plant extract adsorption on the copper surface best fits the Langmuir isotherm.

Figure 7(b) and Table 6 validate the Flory–Huggins adsorption isotherm at 20°C with various concentrations of methanolic plant extract, intended as log θ/C against log $(1-\theta)$. Instantaneously, lines are attained with X as slope and log x K as intercept.

Flory–Huggins' isotherm illustrates the surface coverage degree features of the adsorbate on the adsorbent [39]. Also conveys the viability and naturalness of an adsorption process the value of slope (x) is equal to 0.92, 0.93, 0.97, and 1.03 (Table 6). X adsorbates are number-conquering

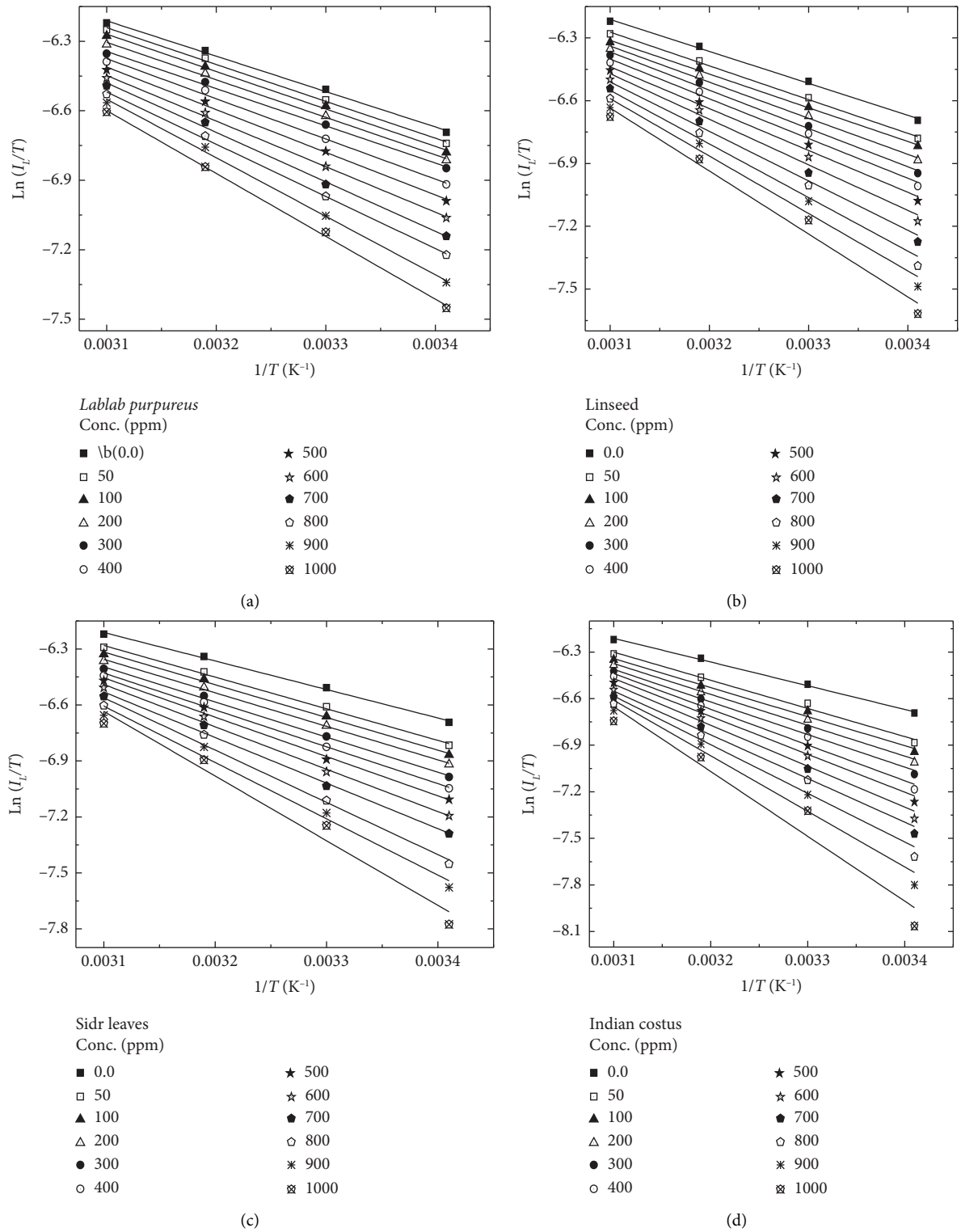


FIGURE 6: Transition state plot of the copper refining in the presence of various concentrations of (a) *Lablab purpureus*, (b) linseed, (c) Sidr leaves, and (d) Indian costus.

adsorption spots. These results could also indicate that four studied methanolic plant extracts dominated one adsorption spot on the copper surface in the electrorefining procedure [33, 39].

Investigational results attained in this research were supplied into the altered Langmuir form isotherm identified as the El-Awady kinetic thermodynamic adsorption model that may properly correspond to the adsorption

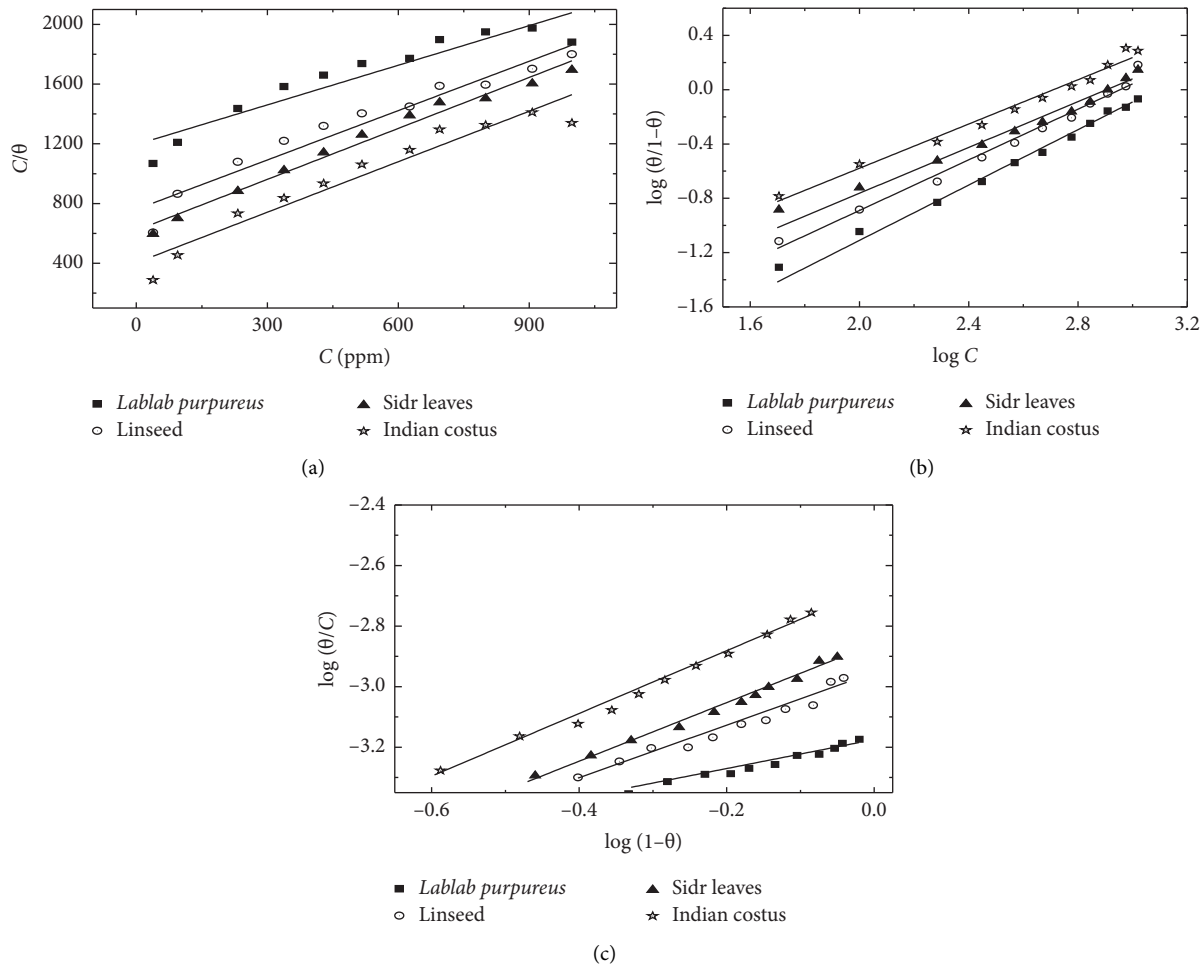


Figure 7: Langmuir, Flory–Higgins, and kinetic–thermodynamic adsorption isotherm at 293 k of the methanolic plant extract.

performance of the examined plant extract onto the copper surface. Plots fitting the investigational data to the kinetic thermodynamic are displayed in Figure 7(c). Straight plots were achieved indicating the authenticity of this model for the four investigated plant extracts. The estimated K, Y, and $1/Y$ values are described in Table 6.

It is noticeable that the values of y equal one entailing that the plant extract employed one adsorption spot on the copper surface.

The $1/y$ values depend on the classification of obstruction matters. From Table 6, it is reasonable that the value of $1/y$ for all plant extract is equal to one suggesting that the plant extract components employed one adsorption spot on the copper surface.

The free energy (ΔG_{ads}) of adsorption at numerous plant extract concentrations is calculated through the subsequent equation:

$$\Delta G_{ads} = -\mathrm{RTIn}\,(55.5\mathrm{K}), \tag{10}$$

where the value 55.5 is the water molar concentration in mol/1.

The negative ΔG_{ads} values demonstrated in Table 6 indicate instinctive adsorption of plant-extracted components on the copper surface and sturdy interaction between the retardation species with the metal surface. The negative (ΔG_{ads}) values are in the range of (3.1–7.5) kJ/mol. It is established that (ΔG_{ads}) implications are > -40, implying that the retardation particles are adsorbed on the copper surface physically [40].

3.8. Surface Characterization via SEM and AFM. It is examined that the surface texture geomorphology was deliberately inspired by the concentration of methanolic plant extract. Figure 8(a) reveals the electrodeposited copper geomorphology in acidified $CuSO_4$ for 5 min at 20°C. Copper species occur as cauliflower-akin to production. It is a permeable, canal composition through which the fine particles' interior might be detected. Refining bath containing 1000 ppm methanolic plant extract reveals a sturdy influence on the microconstruction, i.e., deposit purification (Figures 8(b), 8(c), 8(d), 8(e)) via varying the kind of plant extract attached to the refining bath. The deposit seems eloquently advocated and

Table 6: The K, X, $1/Y$, and ΔG_{ads} values of methanolic plant extract according to Langmuir, Flory–Huggins, and kinetic–thermodynamic isotherm.

Plant extract	Langmuir				Flory-Huggins				Kinetic–thermodynamic isotherm						
	Slope	K	R^2	SD	x	K	R^2	SD	K'	Y	$1/Y$	K	ΔG_{ads} (kJ/mol)	R^2	SD
Lablab purpureus (*Dolichos lablab*)	0.93	8.37×10^{-4}	0.91	0.068	0.92	7.49×10^{-4}	0.92	0.082	7.13×10^{-4}	1.02	0.98	8.24×10^{-4}	−7.51	0.93	0.064
Linseed (*Linum usitatissimum*)	1.13	1.31×10^{-3}	0.92	0.068	0.93	1.30×10^{-3}	0.92	0.082	1.78×10^{-3}	0.94	1.06	1.22×10^{-3}	−6.56	0.93	0.067
Sidr leaves (*Ziziphus spina-christi*)	1.14	1.61×10^{-3}	0.94	0.068	0.97	1.47×10^{-3}	0.95	0.082	5.75×10^{-3}	0.95	1.05	4.44×10^{-3}	−3.41	0.96	0.069
Indian costus (*Saussurea costus*)	1.12	2.47×10^{-3}	0.95	0.068	1.03	2.07×10^{-3}	0.95	0.082	6.19×10^{-3}	0.96	1.04	5.05×10^{-3}	−3.10	0.96	0.075

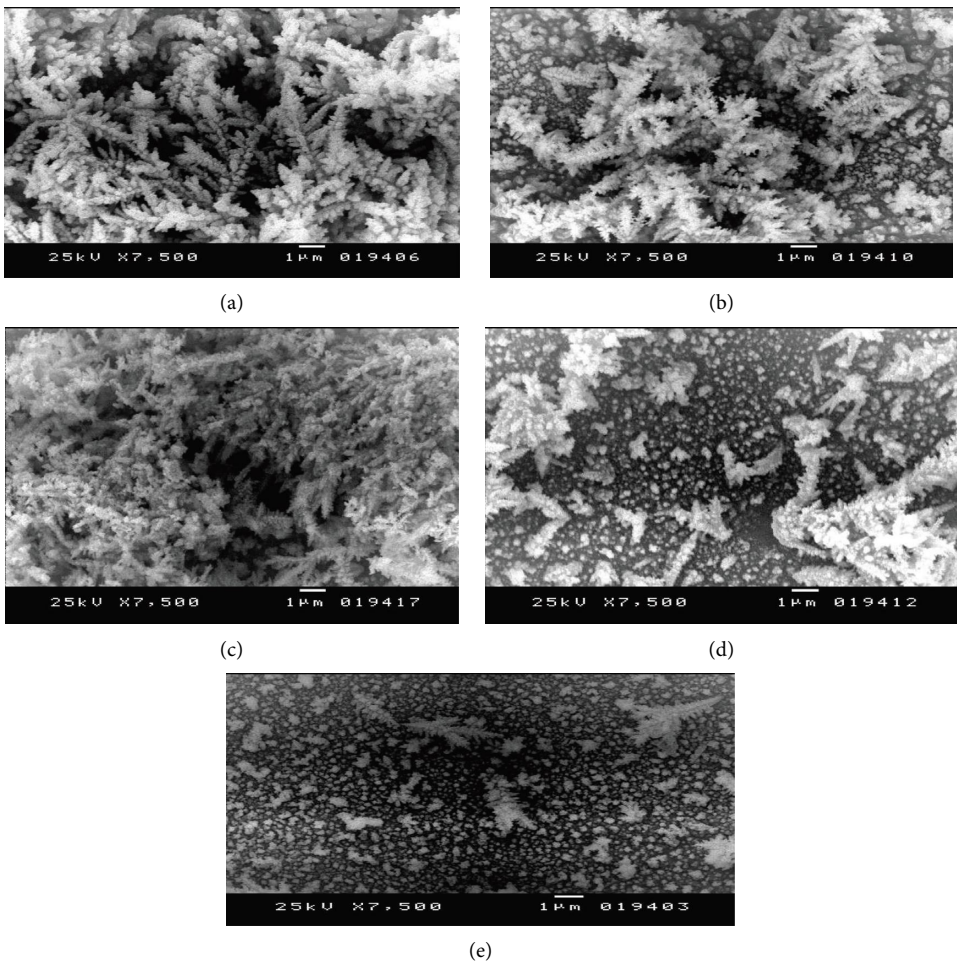


Figure 8: SEM images (a) Blank of copper. (b) After ER + 1000 ppm *Lablab purpureus* (*Dolichos lablab* extract). (c) After ER + 1000 ppm linseed (*Linum usitatissimum*). (d) After ER + 1000 ppm Sidr leaves (*Ziziphus spina-christi*). (e) After ER + 1000 ppm Indian costus (*Saussurea costus*).

regularly wraps the complete electrode surface. In these conditions, expansion is underneath nucleation accomplished via dischargeable classes (Figure 8(b)), while (Figure 8(c)) the deposited layer displays lengthened nonconnected grains arranged in an ordered manner. Adsorption destabilizes the bottom simulated expansion method, and surface unitization directs to the development of insipid geomorphology, over the whole subjugation of advantaged expansion of isolated crystals in the untimely stages of deposition, encouraging structure improvement and surface steamrolling. Figure 8(d) shows regular morphology with the deposit being less uniform and slightly rough. Figure 8(e) shows a smooth surface and the compact coating layer, the deposited organic substituents in Indian costus are powerfully advocated and uniformly cover the entire electrode surface.

The formation of different crystalline structures was observed. This process, known as dendritic growth, occurred due to the electron transfer in the electrode faster than the diffusion of copper ions. The formation of dendrites occurs when the deposition of atoms at the ends of structures facilitates mass transfer and offers less ohmic resistance, resulting in a material with a powdery texture and low adhesion.

Green additives (four investigated plant extracts) may function by changing speciation which changes the reactivity of the metal complex, and accordingly, this changes the redox potential. They can also change the mass transport of species to and from the electrode by changing viscosity which alters the kinetics of growth. Finally, the four investigated plant extracts might adsorb at the electrode solution interface and change the kinetics of nucleation and growth.

Some additives are necessary to develop a coating with the preferred properties [39]. The current work includes the examination of some of these additives. After a series of trials, it was observed that the addition of four investigated plant extracts (1000 ppm) to the bath creates a smooth and bright coating and shows a good leveling effect, especially Indian costus (*Saussurea costus*), found to play a good role in improving the coating thickness too great extent and act as brightening agent since the sample appear brighter. Indian costus has a powerful complexing agent forming a stable complex with copper ions in the bath [41, 42].

To produce copper deposits with proper roughness in electronic applications, it is essential to control the film microstructure. The surface morphology of the matte side

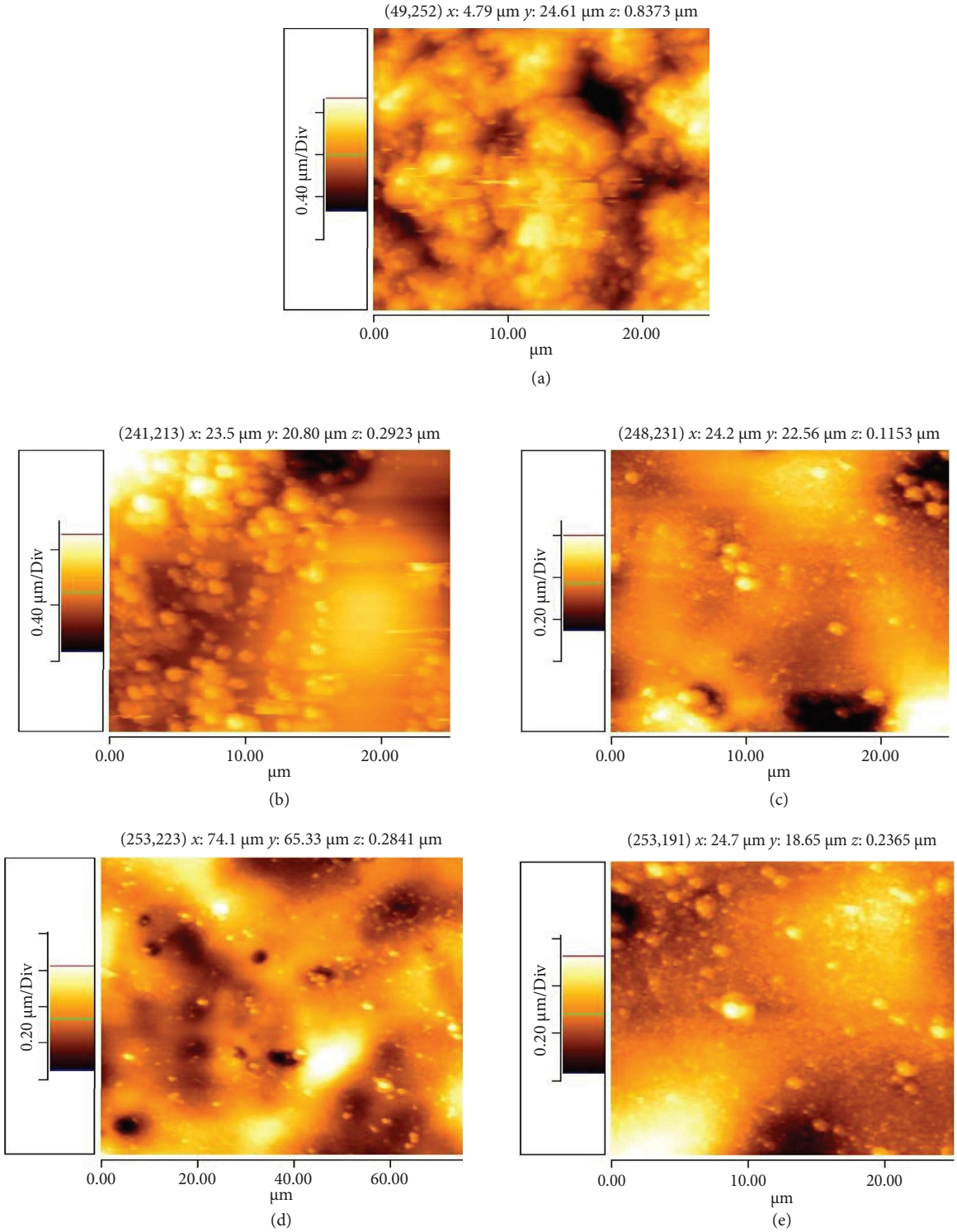


Figure 9: AFM images (a) Blank of copper. (b) After ER + 1000 ppm *Lablab purpureus* (*Dolichos lablab* extract). (c) After ER + 1000 ppm linseed (*Linum usitatissimum*). (d) After ER + 1000 ppm Sidr leaves (*Ziziphus spina-christi*). (e) After ER + 1000 ppm Indian costus (*Saussurea costus*).

of the electrodeposited copper was studied via SEM and AFM. The results are presented in Figure 9. When no additives were present, the film had a rough surface morphology, and the grain structure was more irregular. When plant extract was added to the refining bath, a decreased grain size and a more uniform distribution of grains were obtained (Figure 9). The electrodeposited films were visibly less rough than the film derived without plant extract due to increased coverage of plant extract components adsorption on the cathode surface. The obtained grains with plant extract as the additive were more homogeneously distributed throughout the entire cathode

Table 7: Measured roughness (Ra), Rq (RMS), (PV) peak-to-valley ratio, and reflectance value of copper samples in absent and present natural extracts.

1000 ppm methanolic extract	Blank	*Lablab purpureus* (*Dolichos lablab* extract)	Linseed (*Linum usitatissimum*)	Sidr leaves (*Ziziphus spina-christi*)	Indian costus (*Saussurea costus*)
Ra (nm)	141.9	81.16	70.16	60.48	47.57
Rq (RMS) (nm)	179.5	103.00	87.56	72.58	58.28
PV (nm)	1335	674.3	771	541	438.2

Table 8: In vitro antimicrobial activity by agar diffusion method of the tested compounds.

Natural product	Microorganism inhibition (mm) zone			
	Bacillus subtilis	*Escherichia coli*	*Candida albicans*	*Aspergillus flavus*
Penicillin	50	45	17	46
Lablab purpureus (*Dolichos lablab* extract)	30	29	18	35
Linseed (*Linum usitatissimum*)	40	30	17	40
Sidr leaves (*Ziziphus spina-christi*)	30	30	14	30
Indian costus (*Saussurea costus*)	27	28	12	35

surface. The observations indicate that the presence of plant extract in the electrolyte affects the nucleation and growth of the copper deposit. The nucleation energy for grain formation is expected to decrease, which results in a more uniform surface morphology. The four investigated plant extracts are likely to form a partly covered adsorption layer, which changes the copper reduction and surface roughness of the copper deposit. Plant extract components can be adsorbed onto high surface-energy areas of the cathode such as the edges, nodules, and needles.

AFM was used to resolve the surface roughness of the copper deposit (Figure 9). The grain size and surface roughness gradually decreased, and the leveling and grain refining effect degraded when the different plant extract (1000 ppm) was added, which is attributed to the full coverage and loss of selectivity of adsorption on the protrusions. From an examination of Table 7, it is observed that the blank copper sample records the highest surface roughness (141.92 μm). Oppositely, ER in the solution containing 1000 ppm of plant extract should be very different from the case containing acidified copper sulfate only. Hence, their corresponding surface roughness parameters are mainly decreased to a great extent. Ra value decreases depending on the type of plant extract, where Ra values are 81.16, 70.16, 60.48, and 47.57 nm in the presence of *Lablab purpureus* (*Dolichos lablab* extract), Linseed (*Linum usitatissimum*), Sidr leaves (*Ziziphus spina-christi*), and Indian costus (*Saussurea costus*), respectively. So, the green additives adsorb differently at the electrode–solution interface which changes the deposit morphology. The nucleation mechanism also shows a good leveling effect with an even film thickness [43].

3.9. Biological Activity

3.9.1. Antimicrobial Activity. The diameters of the zone of retardation were calculated and contrasted with that of the standard, and the values are represented in Table 8.

The plant extract substances were examined in vitro for their antimicrobial activities against *Escherichia coli* NRRL B-210 (Gram −ve bacteria), Bacillus subtilis NRRL B-543 (Gram +ve bacteria), Aspergillus flavus, and Candida albicans NRRL Y-477 (fungi).

The conclusions suggested that normally investigated compounds did not appear elevated action contrary to bacteria under investigation (*Escherichia coli* and Bacillus subtilis) while some compounds exposed elevated action against fungi. All plant extracts were active against microorganisms. The antimicrobial screening suggests that all-natural product substances demonstrated mild to great action versus the examined organisms [43].

3.9.2. Antiviral Activity. The antiviral activity of the crude extracts was examined in the postconnection stages of the virus reproduction sequence. It was detected that 100 μg/mL extract should not inhibit the performance of cytopathic influence of HSV-2 in cell culture and 800 μg/mL of extract retard the HSV-2-associated CPE performance in Vero cells. Consequently, the IC50 value for filtered extract is 526 μg/mL, while the SI value for the antiviral activity is 6.04.

The cytotoxicity crude extract on Vero cells was defined by an estimate of CC50 that is 3236, 3222, 3435, and 3323 μg/mL for *Dolichos lablab*, linseed, Sidr leaves, and Indian costus, respectively [44, 45].

3.10. Cathodic Current Efficiency. One of the most significant factors for electrorefining is the current efficiency of the electrode at the cathode. A high cathodic current efficiency is advantageous so that most of the energy going into the electrorefining cell is being used to deposit the metal and is not squandered on side reactions such as hydrogen progression [46]. For these reasons, the CCE of copper deposition from a bath containing plant extract was investigated under different refining conditions. The results are shown in Table 9.

Table 9: The effect of plant extract concentration on the cathodic current efficiency (CCE) of Cu electrorefining.

Natural extract	*Dolichos lablab* (*Lablab purpureus*)					Linseed (*Linum usitatissimum*)				
	W1	W2	*m*	*X*	Current efficiency	W1	W2	*m*	*X*	Current efficiency
Blank	4.167	4.160	0.007	0.036	19.44	4.167	4.160	0.007	0.036	19.44
200	4.124	4.116	0.008	0.032	25.00	4.886	4.878	0.008	0.030	26.67
400	4.544	4.535	0.009	0.029	31.03	4.756	4.747	0.009	0.0265	33.96
600	4.635	4.624	0.011	0.025	44.00	4.322	4.312	0.010	0.0222	45.06
800	4.117	4.105	0.012	0.0214	56.07	4.467	4.456	0.011	0.0181	61.11
1000	4.558	4.545	0.013	0.017	76.47	4.558	4.546	0.012	0.0144	83.33
	Sidr leaves (*Ziziphus spina-christi*)					Indian costus (*Saussurea costus*)				
Blank	4.167	4.160	0.007	0.036	19.44	4.167	4.160	0.007	0.036	19.44
200	4.643	4.635	0.008	0.029	27.58	4.876	4.868	0.008	0.0264	30.30
400	4.256	4.247	0.009	0.0255	35.29	4.454	4.445	0.009	0.0222	40.54
600	4.654	4.643	0.010	0.021	47.62	4.322	4.313	0.009	0.0184	50.00
800	4.788	4.777	0.011	0.017	64.71	4.566	4.556	0.010	0.0144	69.44
1000	4.565	4.554	0.011	0.0123	89.43	4.447	4.438	0.009	0.0095	94.73

The data indicate that the CCE depends on plant extract concentration. The CCE markedly increases with increasing plant extract concentration in the bath from 200 to 1000 ppm. This is attributed to the fact that an increase in Cu content in the bath tends to oppose the depletion of Cu^{2+} ions in the cathodic diffusion layer. Also, the CCE increases with increasing plant extract concentration in the bath due to an increase in the stability of copper–plant extract complex species. This could be attributed to the fact that increasing plant extract content in the bath results in a decrease in the Cu^{2+} deposition in the diffusion layer and consequently decreases the concentration (diffusion) over potential. The presence of plant extract diminishes the hydrogen evolution at the cathode and preserves the energy consumed in agitation [35].

4. Conclusion

- The addition of *Lablab purpureus*, Linseed, Sidr leaves, and Indian costus extract to the electrorefining electrolyte leads to a decrease in limiting current owing to investigated herbal extract controls deposition proportion of copper via rising electrolyte viscosity, which influences their planarization capability.
- The values of activation energies prove that the refining procedure rate was diffusion-checked.
- There is a reduction in the limiting current values via developing plant extract concentration while there is a growth in limiting current values via temperature boosting (293–313 K).
- Adding elevated methanolic plant extract concentration (1000 ppm) to the refining bath is extremely valuable in improving surface features and appears to have a promising influence.
- Langmuir, Flory–Huggins, and the kinetic–thermodynamic model data were established to illuminate the kind of extract adsorption on copper–solution boundary.
- Methanolic plants extract compounds that obey Langmuir, Flory–Huggins, and kinetic–thermodynamic models.
- An endothermic nature was ascribed to positive enthalpy values while the negative entropy values demonstrated a systematic methanolic plant extract adsorption particles on the copper surfaces.
- All plant extracts were active against microorganisms. The antimicrobial screening suggests that all-natural product substances demonstrated mild to great action versus the examined organisms.
- Roughness parameters are mostly decreased. Ra value decreases depending on the type of plant extract.
- Ra values are 81.16, 70.16, 60.48, and 47.57 nm in the presence of *Lablab purpureus* (*Dolichos lablab* extract), Linseed (*Linum usitatissimum*), Sidr leaves (*Ziziphus spina-christi*), and Indian costus (*Saussurea costus*), respectively.
- The CCE markedly increases with increasing plant extract concentration in the bath from 200 to 1000 ppm.

Data Availability Statement

The data used to support the findings of this study are included within the article and its supporting information.

Conflicts of Interest

The authors declare no conflicts of interest.

Funding

There are no funders to report for this submission.

References

[1] J. Y. Hwang, T. Jiang, M. W. Kennedy, et al., "The Minerals, Metals & Materials Series," *9th International Symposium on*

High-Temperature Metallurgical Processing (Cham, Switzerland: Springer Nature, 2018).

[2] W. G. Davenport, M. King, M. Schlesinger, and A. K. Biswas, *Extractive Metallurgy of Copper* (Oxford, UK: Pergamon, 2002).

[3] P. Ashtari and P. Pourghahramani, "Selective Mechanochemical Alkaline Leaching of Zinc From Zinc Plant Residue," *Hydrometallurgy* 156 (2015): 165–172, https://doi.org/10.1016/j.hydromet.2015.03.017.

[4] F. Abouzeid, "Comparison Between Electropolishing Behavior of Copper and Mild Steel in the Presence of Lactic and Mandelic Acid," *International Journal of Electrochemical Science* 11 (2016): 7269–7281.

[5] M. Wang, W. Chen, and X. Li, "Substance Flow Analysis of Copper in Production Stage in the U.S. From 1974 to 2012," *Resources, Conservation and Recycling* 105 (2015): 36–48, https://doi.org/10.1016/j.resconrec.2015.10.012.

[6] L. Yan, A. Wang, Q. Chen, and J. Li, "Dynamic Material Flow Analysis of Zinc Resources in China," *Resources, Conservation and Recycling* 75 (2013): 23–31, https://doi.org/10.1016/j.resconrec.2013.03.004.

[7] M. Wang, W. Chen, and X. Li, "One Year Substance Flow Analysis of Copper Cycle in U.S," in *Proceedings of the Ninth International Conference on Management Science and Engineering Management* (Karlsruhe, Germany: Springer Berlin Heidelberg, July 2015), 1265–1272.

[8] L. Zhang, J. Yang, Z. Cai, and Z. Yuan, "Analysis of Copper Flows in China From 1975 to 2010," *The Science of the Total Environment* 478 (2014): 80–89, https://doi.org/10.1016/j.scitotenv.2014.01.070.

[9] T. Subbaiah, P. SlNGH, G. Hefter, D. Muir, and R. P. Das, "Electrowinning of Copper in the Presence of Anodic Depolarisers-A Review," *Mineral Processing and Extractive Metallurgy Review* 21, no. 6 (2000): 479–496, https://doi.org/10.1080/08827500008914175.

[10] H. H. Abdel-Rahman, A. M. Ahmed, A. A. . Harfoush, and A. H. E. Moustafa, "The Effect of Aromatic and Aliphatic Amines on Copper Electrowinning From Acidic Sulphate Electrolyte," *Hydrometallurgy* 104, no. 2 (2010): 169–177, https://doi.org/10.1016/j.hydromet.2010.05.015.

[11] H. H. Abdel-Rahman, A. A. Harfoush, and A. H. E. Moustafa, "Effect of New Diamine Additives on Rate and Qualities of Nickel Deposition," *Transactions of the IMF* 91, no. 1 (2013): 32–43, https://doi.org/10.1179/0020296712z.00000000061.

[12] H. A. Rahman, A. H. E. Moustafa, and S. A. Magid, "High Rate Copper Electrodeposition in the Presence of Inorganic Salts," *International Journal of Electrochemical Science* 7, no. 8 (2012): 6959–6975, https://doi.org/10.1016/s1452-3981(23)15761-0.

[13] F. M. Abouzeid, "Influence of Vitamin C on Copper Electrorefining From Acidic Solution of Copper Sulfate," *Asian Journal of Chemistry* 27, no. 12 (2015): 4337–4343, https://doi.org/10.14233/ajchem.2015.19119.

[14] A. Murray, H. Khakbaz, A. Pranowo, M. B. Aslin, and M. Bobby Kannan, "Effects of Process Parameters on the Adhesive Strength of Copper Electrodeposits in a Bench-Scale Electrowinning Cell," *Mineral Processing and Extractive Metallurgy* 125, no. 1 (2016): 10–16, https://doi.org/10.1080/03719553.2015.1109183.

[15] E. H. Nkuna, A. P. I. Popoola, O. S. I. Fayomi, and M. G. Kanakana-Katumba, "Experimental Investigation of the Benefits and Process Limitations of Thiourea Dosing in Copper Electrorefining for Improved Cathode Quality," *Current Topics in Electrochemistry* 22 (2020): 51–56.

[16] F. M. Abouzeid and S. Alshammery, "Physico-Chemical Studies of Almond Shell Extracts Potential on the Electropolishing and Electrorefining of Copper," *Asian Journal of Chemistry* 33, no. 10 (2021): 2333–2340, https://doi.org/10.14233/ajchem.2021.23298.

[17] M. A. M. Habib, R. Hasan, J. Nayeem, and N. Uddin, "Rana. Anti-Inflammatory, Antioxidant, and Cytotoxic Potential of Methanolic Extract of Two Bangladeshi Beans *Lablab purpureus* L. Sweet White and Purple," *International Journal of Pharmaceutical Sciences and Research* 3 (2012): 776–781.

[18] A. C. Kudi and S. H. Myrint, "Antiviral Activities on Some Nigerian Medicinal Plant Extracts," *Journal of Ethnopharmacology* 68 (1999): 289–294.

[19] A. Kujumgier, I. Tsevtkova, J. Serkedjieva, V. Bankova, R. Christov, and S. Popov, "Antibacterial, Antifungal, and Antiviral Activity of Propolis of Different Geographic Regions," *Journal of Ethnopharmacology* 64 (1999): 235–240.

[20] M. Cabibbo, H. J. McQueen, E. Evangelista, S. Spigarelli, M. Di Paola, and A. Falchero, "Microstructure, and Mechanical Property Studies of AA6056 Friction Stir Welded Plate Mater," *Materials Science and Engineering: A* 461 (2007): 86–94.

[21] D. Landolt, P. F. Chauvy, and O. Zinger, "Electrochemical Micromachining, Polishing and Surface Structuring of Metals: Fundamental Aspects and New Developments," *Electrochimica Acta* 48, no. 20-22 (2003): 3185–3201, https://doi.org/10.1016/s0013-4686(03)00368-2.

[22] M. H. Kahsay, D. RamaDevi, Y. P. Kumar, et al., "Synthesis of Silver Nanoparticles Using Aqueous Extract of Dolichos Lablab for Reduction of 4-Nitrophenol, Antimicrobial and Anticancer Activities," *Open* 3 (2018): 28–37, https://doi.org/10.1016/j.onano.2018.04.001.

[23] L. de Viguerie, P. A. Payard, E. Portero, Ph. Walter, and M. Cotte, "The Drying of Linseed Oil Investigated by Fourier Transform Infrared Spectroscopy: Historical Recipes and Influence of Lead Compounds," *Progress in Organic Coatings* 93 (2016): 46–60, https://doi.org/10.1016/j.porgcoat.2015.12.010.

[24] A. A. Moosa and M. F. Muhsen, "Ceramic Filters Impregnated With Silver Nanoparticles Household Drinking Water Treatment," *American Journal of Materials Science* 7, no. 6 (2017): 232–239.

[25] R. Vijayan, S. Joseph, and B. Mathew, "Costus Speciosus Rhizome Extract Mediated Synthesis of Silver and Gold Nanoparticles and Their Biological and Catalytic Properties," *Inorganic and Nano-Metal Chemistry* 49, no. 8 (2019): 249–259, https://doi.org/10.1080/24701556.2019.1661439.

[26] F. Abouzeid, A. Taha, M. Elsadek, Y. Elsadek, and Y. M. Othman, "The Electropolishing of C-Steel in Orthophosphoric Acid Containing Methanolic Plant Extract," *Alexandria Engineering Journal* 61, no. 6 (2022): 4889–4909, https://doi.org/10.1016/j.aej.2021.09.058.

[27] T. Zhao, S. J. Li, Z. X. Zhang, et al., "Chemical Constituents From the Genus Saussurea and Their Biological Activities," *Heterocyclic Communications* 23, no. 5 (2017): 331–358, https://doi.org/10.1515/hc-2017-0069.

[28] A. L. Nnanna, O. W. John, E. T. Esihe, C. K. Denkoro, I. V. Okparaku, and O. K. Uchendu, "Inhibitive Effect of Costus After Extracts on Mild Steel Corrosion in Acidic Medium," *International Journal of Engineering and Technologies* 7 (2016): 60–76.

[29] A. M. Basuny, S. M. Arafat, and H. A. Farag, "Utilization from Fruits and Leaves of Nape (Zizyphus Spina–Christi l.) as a Source of Bioactivecomponents," *Banat's Journal of Biotechnology* 6 (2013): 7–16.

[30] A. A. Taha, F. M. Abouzeid, M. M. Elsadek, and Habib, "Effect of Methanolic Plant Extract on Copper Electro-Polishing in Ortho-Phosphoric Acid," *Arabian Journal of Chemistry* 13, no. 8 (2020): 6606–6625, https://doi.org/10.1016/j.arabjc.2020.06.017.

[31] N. Gharda, M. Galai, L. Saqalli, et al., "Linseed Oil as a Novel Eco-Friendly Corrosion Inhibitor of Carbon Steel in 1 M HCl," *Surface Review and Letters* 26, no. 02 (2019): 1850148–1850212, https://doi.org/10.1142/s0218625x18501482.

[32] V. Kavitha and Dr. N. Gunavathy, "Seed Extract of *Lablab purpureus* as Green Corrosion Inhibitor for Mild Steel in 1N Hydrochloric Acid Medium: An Experimental and Computational Investigations," *Journal of Emerging Technologies and Innovative Research* 6 (2019): 64–72.

[33] F. M. Abouzeid and S. Alshammery, "The Hibiscus Extract Potential in Inhibiting Anodic Dissolution of Copper," *Revista de Chimie* 73, no. 3 (2022): 67–81, https://doi.org/10.37358/rc.22.3.8536.

[34] A. A. M. El-Sayed, F. M. Abouzeid, M. M. Ismail, and G. M. Elzokm, "Characterization and Utilization of *Sargassum linifolium* and *Stypopodium schimperi* polysaccharides as Blue Inhibitors for Steel Electo-Polishing," *Water Science and Technology* 83, no. 2 (2021): 409–424, https://doi.org/10.2166/wst.2020.586.

[35] F. M. Abouzeid and H. A. Abubshait, "The Study of Vitamin B Influence on the Morphology, Roughness, and Reflectance of Electropolished Aluminum in H3PO4-H2so4 Mixture," *Arabian Journal of Chemistry* 13 (2020): 2579–2595.

[36] A. A. Taha, F. M. Abouzeid, and M. M. Kandil, "Some Drugs Effect on the Electropolishing of C-Steel in H3PO4 Acid Under Normal and Compulsory Convection Circumstances," *Russian Journal of Electrochemistry* 56, no. 3 (2020): 189–205, https://doi.org/10.1134/s102319352003012x.

[37] F. M. Abouzeid, "Study of Steel Electro-Dissolution Behavior in Presence of Some Surfactants. Electrochemical Investigation and Surface-Active Properties Determination," *Revista de Chimie* 72, no. 3 (2021): 179–197, https://doi.org/10.37358/rc.21.3.8447.

[38] A. M. Abdel-Gaber, H. T. Rahal, and F. T. Beqai, "Eucalyptus Leaf Extract as a Eco-Friendly Corrosion Inhibitor for Mild Steel in Sulfuric and Phosphoric Acid Solutions," *International Journal of Integrated Care* 11, no. 2 (2020): 123–132, https://doi.org/10.1007/s40090-020-00207-z.

[39] S. M. Shaban, M. Elbhrawy, A. Fouda, et al., "Corrosion Inhibition and Surface Examination of Carbon Steel 1018 via N-(2-(2-Hydroxyethoxy)ethyl)-N,N-Dimethyloctan-1-Aminium Bromide in 1.0 M HCl," *Journal of Molecular Structure* 1227 (2021): 129713–129720, https://doi.org/10.1016/j.molstruc.2020.129713.

[40] E. Ituen, O. Akaranta, and A. James, "Evaluation of Performance of Corrosion Inhibitors Using Adsorption Isotherm Models: An Overview," *Chemical Science International Journal* 18, no. 1 (2017): 1–34, https://doi.org/10.9734/csji/2017/28976.

[41] A. A. Taha, H. A. Rahman, F. Abouzeid, and F. M. Abouzeid, "Effect of Surfactants on the Rate of Diffusion-Controlled Anodic Dissolution of Copper in Orthophosphoric Acid," *International Journal of Electrochemical Science* 8, no. 5 (2013): 6744–6762, https://doi.org/10.1016/s1452-3981(23)14801-2.

[42] A. B. Abdel-Aziz, M. M. B. El-Sabbah, I. M. Ghayad, and A. A. El-Zomrawy, "Electroless Plating Lead and Lead-Tin on Copper Using an Eco-Friendly Plating Bath," *Materials Sciences and Applications* 11, no. 12 (2020): 867–879, https://doi.org/10.4236/msa.2020.1112057.

[43] F. M. Abouzeid and S. Alshammery, "Characterization and Utilization of Apple Peel and Grape Stems Extract Constituents as Green Restraints for Aluminum Dissolution," *Scientific Reports* 14, no. 1 (2024): 24170, https://doi.org/10.1038/s41598-024-73592-5.

[44] Z. Keivan, M. A. Zadeh, A. Z. Moloud, S. Kohzad, and R. Zahra, "Antiviral Activity of Aloe Vera Against Herpes Simplex Virus Type 2: An In Vitro Study," *African Journal of Biotechnology* 6, no. 15 (2007): 1770–1773, https://doi.org/10.5897/ajb2007.000-2276.

[45] R. Borges-Argáez, R. Chan-Balan, L. Cetina-Montejo, et al., "In Vitro Evaluation of Anthraquinones From Aloe Vera (Aloe Barbadensis Miller) Roots and Several Derivatives Against Strains of Influenza Virus," *Industrial Crops and Products* 132 (2019): 468–475, https://doi.org/10.1016/j.indcrop.2019.02.056.

[46] M. M. Kamel, A. Abd El-Moemen, M. S. Rashwan, and A. M. Bolbol, "Electrodeposition of Nanocrystalline Copper Deposits Using Lactic Acid-Based Plating Bath," *Metals* 71 (2018): 179–183.